Coordination Chemistry Reviews 561 (2026) 217899

Contents lists available at ScienceDirect

Coordination Chemistry Reviews

journal homepage: www.elsevier.com/locate/ccr

Naphthalimide-based ligands in metal complexes: bridging structural design and biological activity

Julia Stjärnhage [a], Jonathan A. Kitchen [b], Christian G. Hartinger [a,*]

[a] School of Chemical Sciences, University of Auckland, Private Bag 92019, Auckland 1142, New Zealand
[b] School of Science, Auckland University of Technology, Private Bag 92006, Auckland 1142, New Zealand

ARTICLE INFO

Keywords:
Naphthalimide
Metal complexes
Biological properties
Modes of action
Chemotherapy
Photophysical properties
Drug development

ABSTRACT

Metal complexes are a mainstay in cancer chemotherapy since the discovery of cisplatin and related metal complexes as highly effective anticancer agents. Interest in the development of other metal complexes has been driven by the various drawbacks of these agents including their off-target toxicity and tumour resistance. An important strategy towards development of new anticancer metal complexes is through incorporation of organic moieties which themselves have biological activity. Various organic compounds derived from 1,8-naphthalimide have found use in biological applications, with the core scaffold being highly fluorescent and intercalating DNA. As naphthalimide-based organic compounds have reached phase 2 clinical trials, considerable interest was prompted towards utilising the naphthalimide moiety in the design of bioactive metal complexes. Within this comprehensive review, we have collated and described the diverse range of biologically active metal complexes that have been reported which incorporate naphthalimide moieties. We discussed the impact of naphthalimide functionalisation on the biological properties of metal complexes while we critically examined the advantages and the shortcomings of the followed approaches.

Cancer cell lines

451Lu, human cutaneous melanoma; 4T1, murine mammary gland adenocarcinoma; A2780, human ovarian endometrioid adenocarcinoma; A2780R, A2780cisR, A2780/cDDP, human cisplatin-resistant ovarian endometrioid adenocarcinoma; A498, human renal cell carcinoma; A549, human lung adenocarcinoma; A549/cDDP, A549R, A549cisR, human cisplatin-resistant lung adenocarcinoma; CaCo-2, human colon adenocarcinoma; CRL7687, human melanoma-1 (Hs 936.T(C1)); CT26, murine colon adenocarcinoma; HCT116, human colorectal carcinoma; HeLa, human papillomavirus-related cervical adenocarcinoma; Hep-2, human papillomavirus-related cervical adenocarcinoma; HepG2, human hepatoblastoma; HT-29, HT29, human colon adenocarcinoma; KB, human papillomavirus-related cervical adenocarcinoma; KHOS-NP, human osteosarcoma; LS180, human colon adenocarcinoma; MCF-7, human invasive breast carcinoma; MDA-MB-231, human breast adenocarcinoma; NCI-H460, human non-small-cell lung carcinoma; SiHa, human cervical squamous cell carcinoma; SKOV-3, human ovarian serous cystadenocarcinoma; U937, human acute monocytic leukaemia; WM3918, human melanoma.

Healthy cell models

Abbreviations: ATP, adenosine triphosphate; biPh, biphenyl; bipy, bipyridine; Bn, benzyl; BODIPY, 4,4-difluoro-4-bora-3a,4a-diaza-s-indacene; BSA, bovine serum albumin; Bu, butyl; Cp, η^5-cyclopentadienyl; Cp*, η^5-pentamethylcyclopentadienyl; ct, calf thymus; cym, η^6-*p*-cymene; DFT, density-functional theory; DMSO, dimethyl sulfoxide; DNA, 5-deoxyribonucleic acid; EPR, electron paramagnetic resonance; Et, ethyl; EtBr, ethidium bromide; G4, G-quadruplex; h, hour(s); HIF-1, hypoxia-inducible factor-1; IC_{50}, concentration causing 50% growth inhibition; *i*-Pr, isopropyl; kg, kilogram(s); LD_{50}, median lethal dose; *m*-Ph, meta-phenylene; MAPK, mitogen-activated protein kinase; Me, methyl; mg, milligram(s); mor, morpholine; MLCT, metal-to-ligand charge-transfer; mL, millilitre(s); MMP, mitochondrial membrane potential; mt, mitochondria(l); MTT, 3-(4,5-dimethylthiazol-2-yl)-2,5-diphenyltetrazolium bromide; MYLK, myosin light-chain kinase; n.a., not applicable; NCI, National Cancer Institute; NHC, *N*-heterocyclic carbene; nm, nanometre(s); NP, nanoparticle; PACT, photoactivated chemotherapy; PAMAM, poly (amidoamine); PBS, phosphate buffered saline; PDT, photodynamic therapy; PEG, poly(ethylene glycol); Ph, phenyl; phen, phenanthroline; ppr, piperidine; PPI, poly (propylene imine); Pr, propyl; PS, photosensitiser; PTA, 1,3,5-triaza-7-phosphaadamantane; Py, pyridine; pyr, pyrrolidine; RF, resistance factor; ROS, reactive oxygen species; RTK, receptor tyrosine kinase; stDNA, salmon testes DNA; *t*-Bu, tert-butyl; TAP, 1,4,5,8-tetraazaphenanthrene; TFA, trifluoroacetate; TfO, triflate; tol, η^6-toluene; TOP, topoisomerase; µg, microgram(s); µM, micromole(s) per litre.

* Corresponding author.
E-mail addresses: julia.stjarnhage@auckland.ac.nz (J. Stjärnhage), jonathan.kitchen@aut.ac.nz (J.A. Kitchen), c.hartinger@auckland.ac.nz (C.G. Hartinger).

https://doi.org/10.1016/j.ccr.2026.217899
Received 29 January 2026; Accepted 25 March 2026
Available online 7 April 2026
0010-8545/© 2026 The Authors. Published by Elsevier B.V. This is an open access article under the CC BY-NC license (http://creativecommons.org/licenses/by-nc/4.0/).

BEAS-2B, human bronchial epithelial cell; CA-M75, skin melanocyte; FF2508, human fibroblast; FOM102010, human melanocyte; HEK293, human embryonic kidney cell; NIH, NIH-3T3, human embryonic stem cell; NRK, normal rat kidney cell; PBMC, peripheral blood mononuclear cell.

Bacteria and fungi

A. calcoaceticus, *Acinetobacter calcoaceticus*; *B. cereus*, *Bacillus cereus*; *B. subtilis*, *Bacillus subtilis*; *C. lipolytica*, *Candida lipolytica*; *E. coli*, *Escherichia coli*; *K. pneumoniae*, *Klebsiella pneumoniae*; *S. aureus*, *Staphylococcus aureus*; *S. cerevisiae*, *Saccharomyces cerevisiae*.

1. Introduction

1,8-Naphthalimide (Fig. 1) is a rigid, planar π-deficient aromatic system with the core scaffold fluorescing blue in solution [1], and with a variety of applications due to its structural, physicochemical and biological properties. Non-biological uses mainly rely on the photophysical properties, such as in fluorescent probes, Lucifer dyes, and non-biological sensors [2]. They have also been developed as 'turn-on' chemosensors for various metal ions in biological and non-biological systems [3–5]. Naphthalimide derivatives can carry a wide range of medicinal properties, with agents synthesised that are antiparasitic, antiviral, analgesic/local anaesthetic, and anti-amyloid, as well as compounds that can be used as chemosensors or serotonin receptor antagonists [2,6–8], to name a few.

Naphthalimide fluorescence originates from photoinduced electron transfer within the aromatic system. Hence, compounds in which the naphthalimide structure is incorporated for its fluorescent properties most commonly feature the naphthalimide receptor site substituted at R^4 (Fig. 1). Alternatively and to a lesser extent, R^3 can be derivatised, while R^N substitution can result in an excited state that places a partial negative charge on N(12), which disfavours photoinduced electron transfer [10]. However, several R^N-substituted fluorescent compounds have been reported [11]. By an extension of these fluorescence-quenching conditions, naphthalimides find use in cleavage-based sensors. These connect a fluorescence-quenching moiety *via* a linking receptor that undergoes cleavage in the presence of the target chemical species, thus restoring the fluorescence of the parent naphthalimide structure [12].

2. Naphthalimide-based organic anticancer compounds

The naphthalimide moiety is an efficient DNA intercalator, with the rigid, planar, aromatic structure able to insert between stacked base pairs and to target DNA with high efficiency, even in competitive media under biological conditions where other molecules present can also interact favourably [6]. Many DNA intercalators are cytotoxic, but intercalation alone usually does not result in cell death without other contributing mechanisms, typically from those that directly cause structural damage to DNA or otherwise inhibit normal function, such as antitumour antibiotics that often inhibit topoisomerase 2 (TOP2) [13].

With the core scaffold being a very potent intercalator, relatively small variations can produce derivatives with cytotoxic activity, and several compounds of this type have been developed as anticancer agents [6,14,15]. Mitonafide and amonafide (Fig. 2) were the first two anticancer naphthalimides developed, both progressing to phase II clinical trials in the 1990s [16,17]. They were initially described in the early 1970s by Braña and in the early 1980s were found to be mono-intercalators with cytotoxicity in HeLa and KB cancer cell lines [2,7]. After intercalation, amonafide and mitonafide cause DNA damage by acting as TOP2 poisons. Amonafide disturbs the cleavage and re-ligation equilibrium, causing irreparable DNA-TOP2 adducts to accumulate, while mitonafide inhibits DNA synthesis and induces TOP2-mediated double-strand breaks [6].

Compounds derived from amonafide typically have dual action as TOP2 inhibitors and DNA intercalators, with the combination of intercalation and stabilisation of the DNA-intercalator complex crucial to enact irreparable DNA damage and achieve cytotoxicity [6,18]. In contrast to classic TOP2 poisons, the DNA damage induced by amonafide derivatives is ATP-independent and thus unimpacted by the most common mechanism by which cancer cells become resistant to TOP2 poisons [19]. The cytotoxic mechanism is less due to unrepairable DNA damage compared to classic TOP2 poisons and instead more from antiproliferative effects *via* stabilisation and thus accumulation of DNA-TOP2 adducts, which could further circumvent typical drug resistance mechanisms [20].

Along with developing amonafide, Braña et al. also reported a series of bisnaphthalimides in the 1990s, all of which were bis-intercalators with stronger DNA binding and higher cytotoxicity than their mono-naphthalimide equivalents [21–23]. One of these bisnaphthalimides was elinafide (Fig. 2), which progressed to phase II clinical trials [22–25]. Bisnafide (Fig. 2) is a structurally similar compound, and the mesylate formulation was investigated in phase II clinical trials [26–28] with the mechanism of action also being DNA intercalation and inhibition of TOP2 [29–32]. Elinafide was found to bind to the major groove of DNA in a two-step process, with the cationic aminoalkyl linker chain first forming hydrogen bonds with the guanine bases, after which both naphthalimide moieties intercalate [33,34]. The naphthalimide groups can also exchange by rotational ring flipping while remaining bound and preserving the H bonding, an uncommon phenomenon in intercalated systems that potentially relates to its high sequence selectivity as well as its enhanced cytotoxicity, as more severe topological strain is induced in DNA upon binding (Fig. 3) [35]. DNA intercalators like elinafide and amonafide preferably bind to GC-rich regions of DNA, but naphthalimide derivatives with affinity for other regions have been reported [36–38].

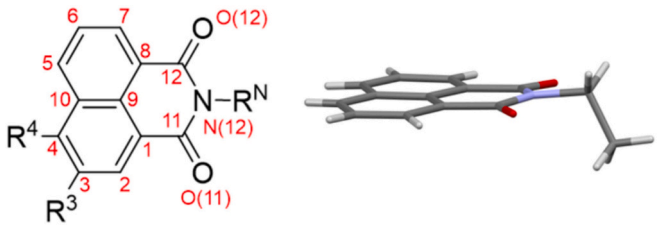

Fig. 1. (left) Chemical structure of the 1,8-naphthalimide scaffold with common substitution sites R^N, R^3, and R^4. (right) Side view of the molecular structure of an N-ethyl derivative demonstrating the planarity of the naphthalimide ring structure (R^3/R^4 = H, R^N = CH_2CH_3) [9].

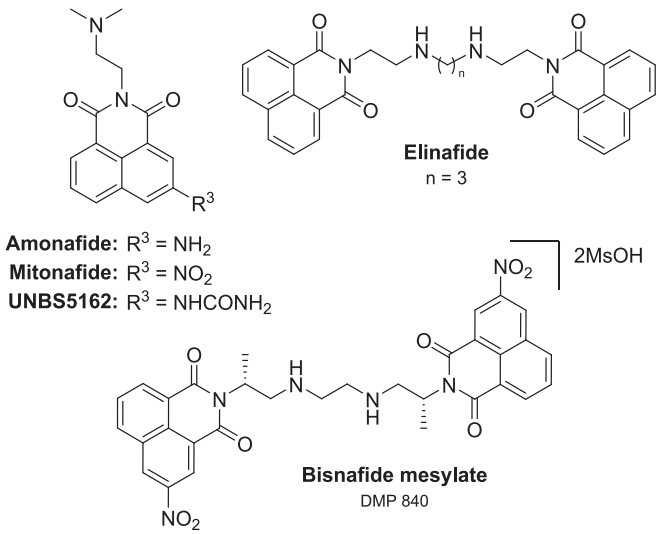

Fig. 2. Naphthalimide anticancer agents that progressed to clinical trials.

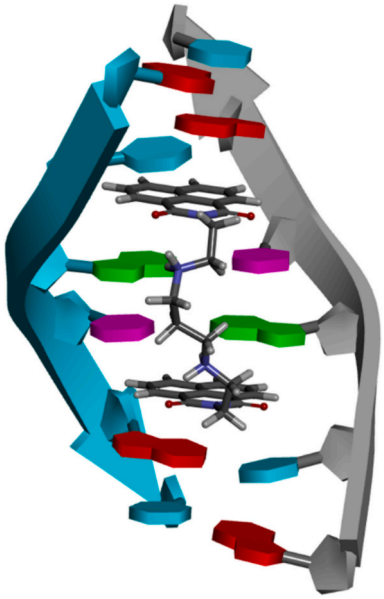

Fig. 3. Solution structure of elinafide intercalated into a d(ATGCAT)$_2$ DNA oligonucleotide. Modified from [35] (PDB ID 1CX3).

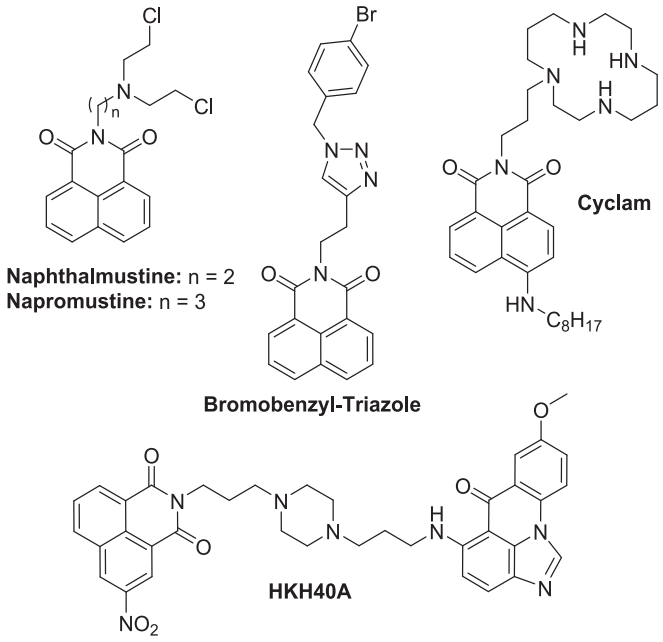

Fig. 4. Bifunctional naphthalimide derivatives with anticancer properties.

The most recent naphthalimide-based anticancer agent reaching clinical trials is UNBS5162 (Fig. 2), an amonafide derivative with a modified R^3 moiety that circumvents a metabolic mechanism that produces a haematotoxic metabolite [39]. With its novel mode of action it shows activity in the NCI60 cell line panel different to that of other agents, including amonafide.

Small N-based substitutions at R^3 and R^4 often increase the cytotoxicity of monofunctional naphthalimide-based compounds, with LC_{50} (median lethal dose) values trending towards a correlation between the substituted and non-substituted compounds. That is, if the non-substituted compound was non-cytotoxic, these substitutions commonly did not increase cytotoxicity significantly [6,40]. Variations at the R^3 and R^4 positions of the naphthalimide core have very different implications for the overall geometry of the compound. A substituent at R^4 is positioned out-of-plane relative to the naphthalimide, whereas one at R^3 lies closer to the plane of the aromatic structure and thus the molecule intercalates into DNA more efficiently with stronger overall binding [6].

In an alternative approach, compounds combining the intercalative naphthalimide structure with a secondary cytotoxic moiety were developed, equipping the compounds with more than one mode of action. These include some of the earliest bifunctional naphthalimide agents that belong to the nitrogen mustards, with naphthalmustine and napromustine (Fig. 4) constituting the first examples [41–45]. Following these early developments, various bifunctional naphthalimide anticancer agents have been successfully designed. A dual inhibitor of topoisomerase 1 (TOP1) and TOP2 based on cyclam (Fig. 4) was synthesised and shown to possess significant *in vitro* cytotoxicity in human cancer cells [46–48]. Organic cyclam compounds do not commonly show anticancer properties [49], and the development of a cytotoxic cyclam-naphthalimide conjugate shows the potential of the naphthalimide moiety even in combination with less strongly cytotoxic components.

Another significant subgroup of bifunctional naphthalimides consists of those conjugated to a second aromatic heterocyclic substituent. HKH40A (Fig. 4) carries an imidazoacridone moiety and although it showed poor aqueous solubility and was subject to degradation in solution under ambient light, it was highly potent in inducing apoptosis of p53-positive cancer cells [50]. Various naphthalimide conjugates with other biologically active aromatic heterocycles were reported. For example, bromobenzyl-triazole (Fig. 4), a conjugate featuring a 1,2,3-triazole linker, showed promising anticancer activity but a poor solubility profile [51]. Other aromatic groups conjugated to naphthalimide to form cytotoxic agents include coumarin [52], indomethacin [53], a non-steroidal anti-inflammatory drug, and various organoselenocyanates [6]. Cyclic aromatic groups, such as furan, thiophene or thiazole, can also be fused directly onto the naphthalimide ring structure yielding compounds with anticancer activity. A thiazole derivative was reported as a lead preclinical agent for the treatment of hepatocellular carcinoma [54,55].

3. Anticancer metal complexes with naphthalimide-substituted ligands

While naphthalimide compounds as monofunctional agents did not have considerable success as selective cytotoxic agents, in part due to the toxicity of early lead compounds, they have demonstrated significant potential as building blocks in multimodal systems [6]. As shown for the bifunctional organic naphthalimide compounds, the naphthalimide moiety can retain the DNA-targeting and -intercalating properties when conjugated to other organic functional groups in bifunctional compounds, while avoiding interactions with metabolic pathways which yield toxic species [1,56–59]. Hence, they were also explored conjugated to biologically active metal complexes. Naphthalimide lacks metal coordination capability, hence most derivatives need to be equipped with a coordinating group at the R^N, R^3, or R^4 positions, in some cases with a second organic, bioactive moiety as the coordinating component. The naphthalimide moiety adds targeting capability towards DNA to the active cytotoxic moiety. As pointed out before, small substituents at R^3 and R^4 can significantly influence the DNA binding affinity of naphthalimide. Furthermore, larger substituents can drastically change or potentially completely quench the activity of the moiety. Thus, substitution at R^3 or R^4 to attach the moiety to a second ligand moiety may result in less effective compounds than R^N-substituted chelating moieties [6,60].

Once coordinated to a metal system, the naphthalimide-functionalised ligand forms part of a multimodal and multitargeted complex, with the inclusion of the naphthalimide moiety often aiming to target DNA. Although the first complexes described in literature featured platinum centres, the scope has more recently been expanded

to ruthenium, copper, and other metals. Selected metal complexes functionalised with naphthalimides were recently reviewed with a focus on imaging applications [61]. Here, we provide a comprehensive review of biologically active coordination and organometallic compounds with a focus on structural features of naphthalimide-functionalised metal complexes with anticancer properties and compounds showing antibacterial potency or activity against other microorganisms (for a structural overview and design rationales of metal complexes functionalised with naphthalimides see Tables S1, S2, S5–S7, S9–S11).

3.1. Platinum in cancer treatment

Metal-based anticancer agents gained significant interest after the discovery of the potency of the Pt(II) complex cisplatin *cis*-[diamminedichloridoplatinum(II)] in the 1960s. Cisplatin and its closely related compounds oxaliplatin and carboplatin target DNA and are used either alone or in combination with other agents to treat a wide range of cancers [62]. However, despite their success, there are a range of concerns associated with their use, including most prominently acquired and intrinsic resistance as well as significant off-target effects and systemic toxicity. Hence, there has been and continues to be significant interest in developing variants of the established Pt(II) agents which can circumvent these issues.

3.1.1. Naphthalimide functionalisation of Pt(II) complexes

The first naphthalimide-substituted anticancer metal complexes were the Pt(II) coordination compounds **NN-1a** and **NN-1b** (Fig. 5; Table S3) as structural variants of cisplatin and carboplatin. These bear ligands closely related to elinafide and were initially described by Braña and Navarro-Ranninger [59]. The ligands coordinate to the metal centre in a bidentate fashion forming a 5-membered ring and replacing the typical ammine ligands which feature in the classic Pt drugs. **NN-1a** and **NN-1b** were designed for the naphthalimide to act as a carrier to improve the DNA targeting of the Pt complex, thus reducing off-target effects and the required dosage. The ligand and Pt moiety acted synergistically to give the complexes higher cytotoxicity than would be expected from an additive mode of action, and also retained the activity in cisplatin-resistant cell lines. This may be due to augmenting effects of DNA platination and naphthalimide intercalation, as both agents act on DNA but enacted damage through different molecular mechanisms.

Other Pt complexes utilising the naphthalimide moiety are the *trans*-Pt complexes **N-1a**–**N-1f** (Fig. 6) which were reported by Quiroga et al., featuring a monodentate *N*-coordinated naphthalimide ligand in *trans*-position relative to a secondary or tertiary aliphatic amine [56]. **N-1a** and **N-1b** showed higher cytotoxicity than cisplatin, with sub-micromolar IC_{50} values in A2780 cells and low resistance factors (RF, ratio IC_{50} resistant cell line: IC_{50} parent cell line), with the compounds displaying sub-micromolar IC_{50} values in cisplatin-resistant A2780cisR cells. DNA binding studies showed that the naphthalimide-enhanced compounds disrupted plasmid DNA more than would be expected from platination alone, as seen with cisplatin. In particular, a decrease in UV–vis absorbance of **N-1b** subsequent to the addition of calf thymus DNA (ctDNA) suggested a contribution of other DNA binding modes

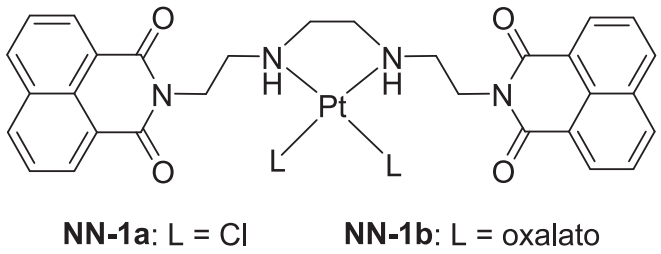

Fig. 5. Chemical structures of the elinafide-based cisplatin and oxaliplatin derivatives **NN-1a** and **NN-1b**.

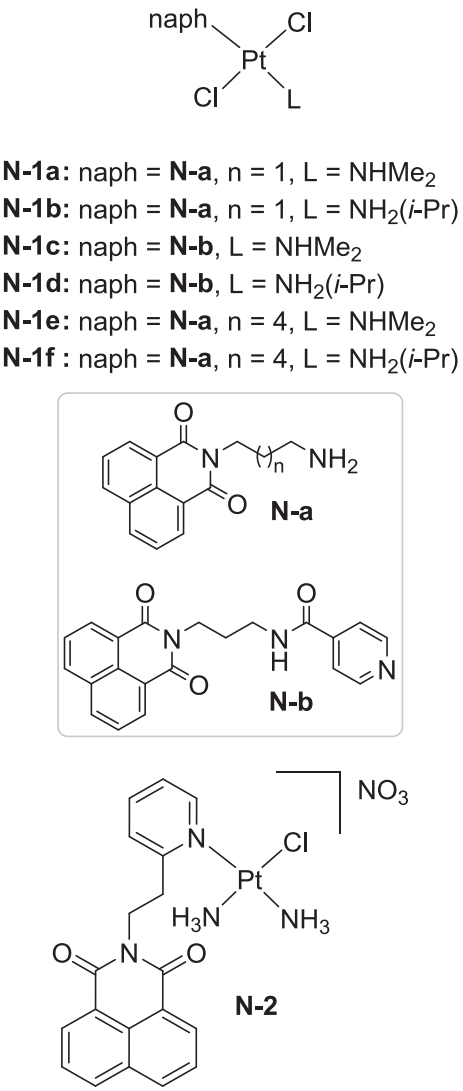

Fig. 6. Chemical structures of *trans*-Pt complexes **N-1a–N1f** and mtDNA targeting complex **N-2**.

through the naphthalimide ligand. Pyridyl-coordinated **N-1c** and **N-1d** were similarly cytotoxic as **N-1e** and **N-1f**, respectively, but with moderately lower RF values. **N-1a** and **N-1b** being more potent than the other compounds in the series suggests that shorter linkers might be more favourable for a combined mode of action of intercalation and platination. The complexes with shorter linkers had better cell uptake compared to **N-1f**, with **N-1b** having a particularly high Pt content in respect to the dose applied. However, while **N-1b** had the highest cellular uptake overall and was the most cytotoxic compound, it was not found to localise to a significantly extent in cellular nuclei, suggesting the mechanism of action does not involve platination of nuclear DNA.

In compound **N-2** (Fig. 6), a chlorido ligand of cisplatin was substituted for an *N*-coordinated monodentate naphthalimide ligand [63]. Compared to cisplatin, **N-2** showed higher cytotoxicity in cancer cell lines while being less cytotoxic towards non-cancerous cells. In *in vitro* murine studies with MCF-7 xenografts and treatment with **N-2** or cisplatin over 15 days at 2.5 mg Pt kg^{-1}, the tumour size decreased significantly more for **N-2** and the LD_{50} value was approximately twice that of cisplatin. Intercalative binding between **N-2** and DNA was observed, which was not found for a reference compound lacking the naphthalimide. Cellular uptake and distribution were moderately increased for **N-2** compared to cisplatin, as was the extent of DNA damage on a single cell level. Alongside inhibiting the repair of DNA, the

compound also induced damage to mitochondria and mitochondrial DNA (mtDNA).

Complexes **NNN-1a** and **NNN-1b** (Fig. 7) feature tridentate chelating moieties restricting the formation of cross-links between DNA strands solely by Pt coordination [64]. Despite this, both complexes showed sub-micromolar cytotoxicity against cancer cell lines, maintained cytotoxicity in cisplatin-resistant cells, and were significantly less active in non-cancerous cells. Although similarly cytotoxic, the two compounds showed preference for binding to different sections of DNA, which may be related to the sterics of interaction defined by the naphthalimide substitution of the different N atoms. **NNN-1b** generally showed less discriminative binding over the DNA structures tested, binding significantly to various guanine sites (Fig. 7).

Polypyridyl complexes are known as photosensitisers (PSs) and have been studied for photodynamic therapy (PDT) [65]. Functionalisation with naphthalimide may change the properties of such complexes. The Pt(II) terpyridyl complex **N-3** (Fig. 8) showed luminescence that originated at the naphthalimide moiety [66] despite its R^N substituent, which can act as a quencher [10]. **N-3** was cytotoxic towards malignant cells and significantly greater DNA-binding affinity was observed than found for polypyridyl complexes [66] and DNA damage was identified as the reason for the biological activity.

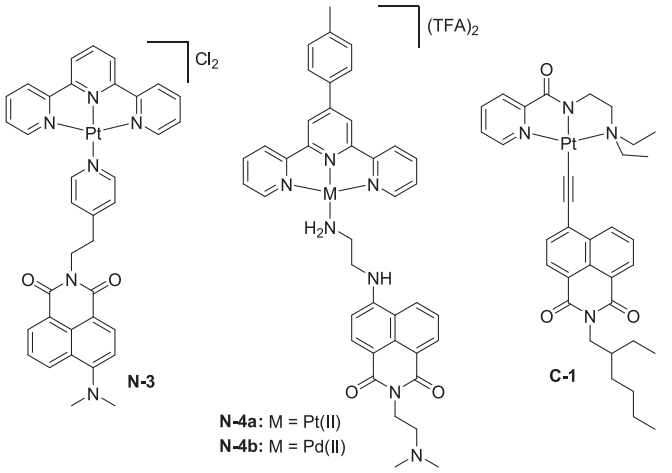

Fig. 8. Structures of the terpyridine Pt or Pd anticancer agents **N-3**, **N-4a** and **N-4b** and photosensitising **C-1** (TFA = trifluoroacetate).

As **N-3**, the Pt agent **N-4a** and its Pd counterpart **N-4b** (Fig. 8) feature a terpyridyl ligand but the naphthalimide moiety is coordinated to the

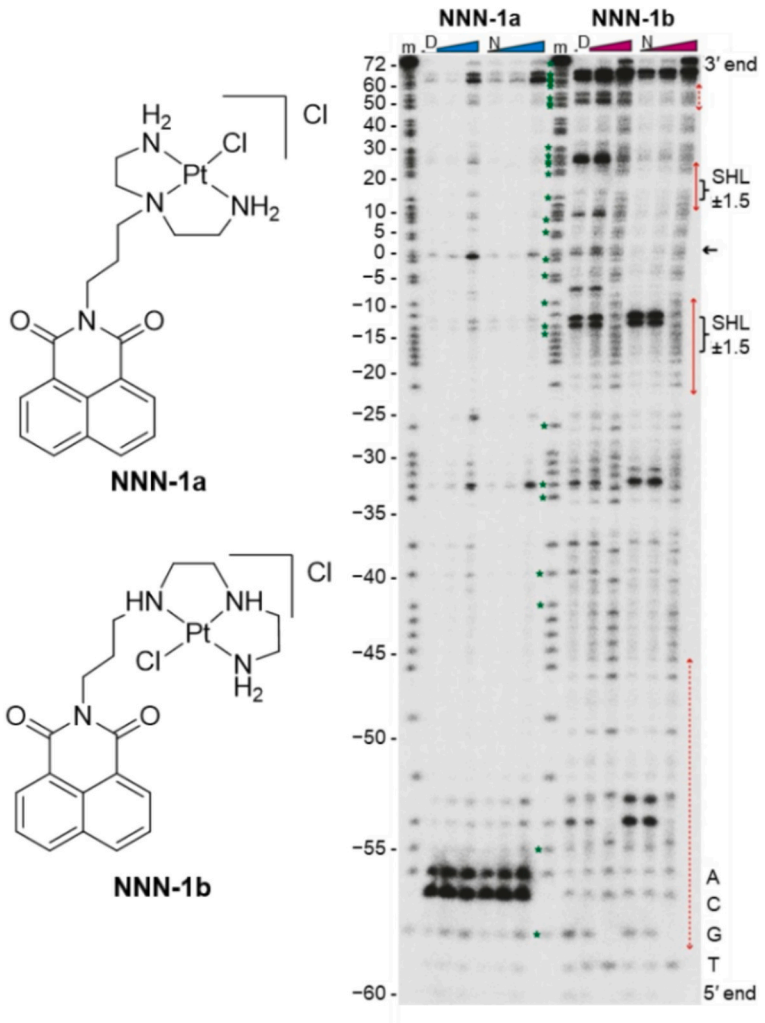

Fig. 7. (Left) Structures of **NNN-1a** and **NNN-1b**, and (Right) their DNA adduct formation profiles with the nucleosome core particle (N) or DNA (D) treated with 10-, 20- or 50-fold excess of **NNN-1a** and 5-, 10- or 50-fold excess of **NNN-1b**; shown are purine sequencing standards (m), numbers represent general nucleotide position relative to nucleosome centre (black arrow), green asterisks designate locations of guanine nucleotides, red arrows indicate regions of DNA stretching in N (solid) and alternative configurations available (dashed). Modified from [64] with permission from Oxford University Press © 2015. (For interpretation of the references to colour in this figure legend, the reader is referred to the web version of this article.)

metal centre through an aliphatic amine rather than a pyridyl [67]. Both complexes were found to bind strongly and selectively to G4 (Fig. 9), which are secondary structures formed by guanine-rich DNA sequences. The association constant was determined by UV–vis spectroscopy and was several orders of magnitude higher than found with ctDNA. Both complexes were more cytotoxic than cisplatin, with **N-4a** also showing higher activity in the cancer cell line than the non-cancerous cell line.

In contrast to the terpyridyl compound **N-3**, **C-1** (Fig. 8) is a PS but does not interact with DNA [68]. When evaluated in two non-small-cell lung cancer cell lines, MCF-7 and A549, as well as the cisplatin-resistant variant of the latter, it was found to be most cytotoxic to the cisplatin-resistant cells and even more so under hypoxic conditions. When irradiated, an IC_{50} value of 0.18 μM was found which was a 44-fold improvement compared to dark conditions, and in general photoirradiation resulted in potent activity which shows potential for the compound to be used even in hypoxic environments where the classic ROS-producing PS typically fails.

OO-1 (Fig. 10) was designed in an approach to conjugate bioactive moieties to the carboplatin core structure [69]. In **OO-1**, naphthalimide was incorporated for its fluorescence rather than DNA targeting, as biotin was intended to act as the tumour-targeting fragment. Biotin can act as a vector to improve selectivity for cancerous tumours through recognition by various biotin-specific receptors on the cell surface overexpressed by rapidly proliferating cells [70–72]. Although **OO-1** was less cytotoxic than cisplatin in A2780 and A549 cells, it had a higher cytotoxicity in the resistant cell lines A2780/cDDP and A549/cDDP with RF values of 2.81 and 1.84, respectively. UV–vis spectroscopy studies showed that the compound underwent changes in the spectrum over 12 h at pH 6.2, resembling the tumour microenvironment, suggesting cleavage of the imine bond. The compound was further found to bind to two proteins which are important for repairing double-strand breaks in DNA and did so more strongly than cisplatin or carboplatin (Fig. 10).

Strictly speaking from a structural point of view, the Pt(II) agents **N-5a**–**N-5f** (Fig. 11) are not naphthalimides but instead benzimidazole derivatives thereof, with part of the scaffold resembling the heteroaromatic ring system of camptothecin [73]. A large variability in the cytotoxic activity of the complexes against various cancer cell lines was observed and **N-5a** was the only compound with activity in all cell lines, including in cisplatin-resistant cell lines. **N-5a** was confirmed to inhibit TOP1 at 40 μM, and affected TOP1 expression *in vitro* at low μM concentrations. *In vivo* mouse studies using NCI-H460 xenografts showed greater inhibition of tumour growth than cisplatin at a 4 mg/kg dose, with no noted toxicity nor adverse effects within the 13-day treatment period.

3.1.2. *Pt(IV) complexes – Activation by reduction*

To overcome the high rate of off-target effects seen in the clinically

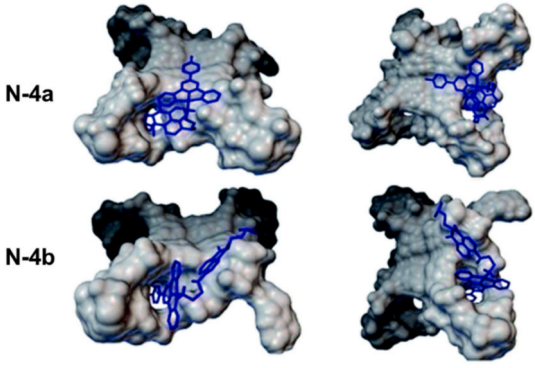

Fig. 9. Molecular docking of **N-4a** (top) and **N-4b** (bottom) with Htelo quadruplex DNA, a telomeric G4-quadruplex structure. Modified from [67] with permission from RSC © 2016.

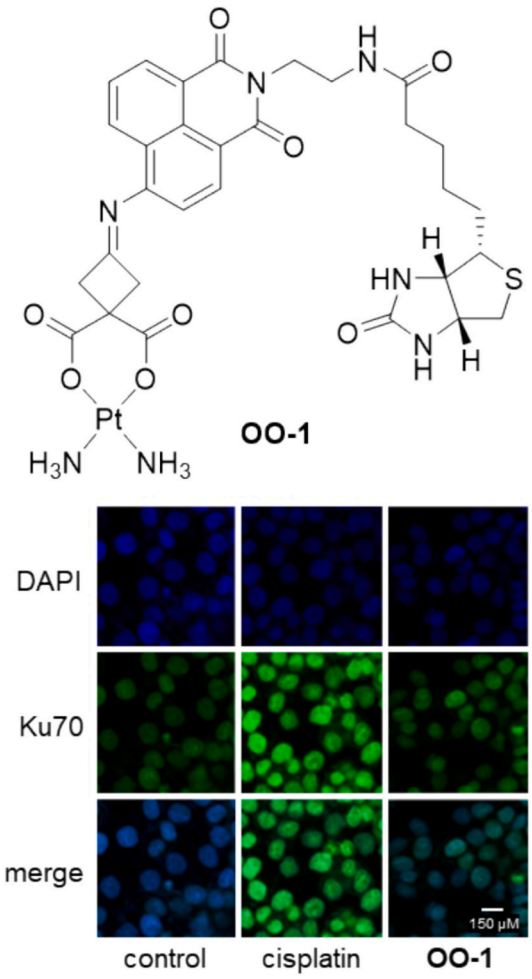

Fig. 10. (Top) Structure of the biotin derivative **OO-1**. (Bottom) Immunofluorescence staining determination of Ku70 expression in A549 cells exposed to **OO-1** (40 μM) for 12 h in comparison to the control and cisplatin (40 μM). Modified from [69] with permission from Elsevier © 2020.

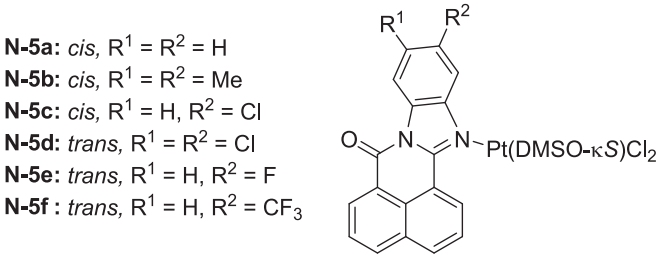

Fig. 11. Structure of naphthalenebenzimidazole compounds **N-5a–N-5f**.

used Pt(II) compounds, kinetically stable Pt(IV) prodrugs have been explored that can be reduced to the respective Pt(II) complexes under hypoxic conditions to release the two axial ligands [74,75]. The Pt(IV) complex **O-1** was designed to release its fluorescent naphthalimide ligand upon reduction in the hypoxic tumour environment, enabling visualisation of hypoxic areas and tracking of treatment. When exposed to HCT116 cells in increasingly hypoxic environments, **O-1** was reduced and gave progressively higher fluorescence emission (Fig. 12) [76]. While it was found to be cytotoxic, no IC_{50} values were calculated. However, incubation of the cells with **O-1** resulted in a lower fraction of cells surviving under hypoxic than normoxic conditions.

Similarly, **O-2a**–**O-2e** (Fig. 13; Table S4) are a series of oxaliplatin-

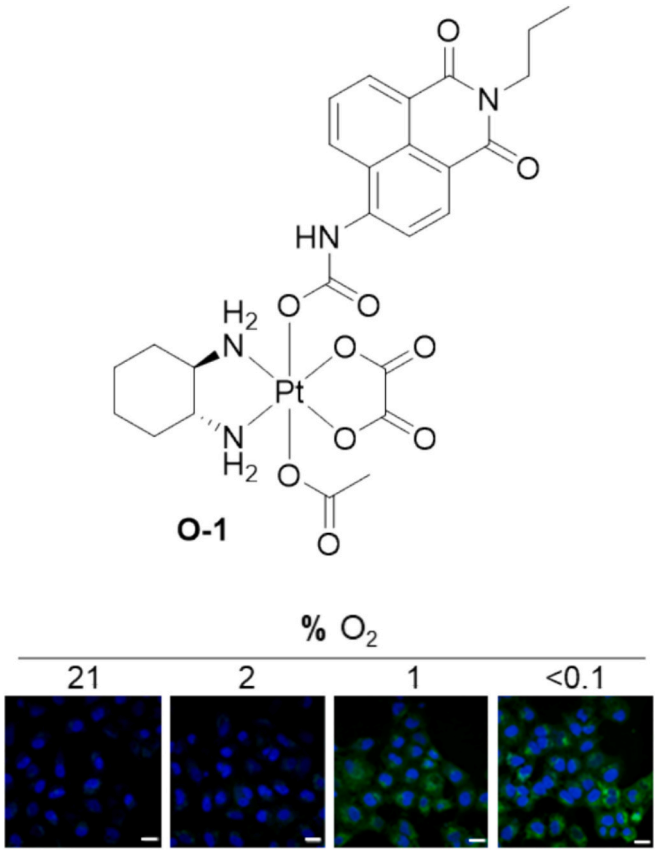

Fig. 12. Structure of hypoxia-fluorescent Pt(IV) oxaliplatin prodrug **O-1** and fluorescence of HCT116 cells treated with **O-1** (10 μM) for 6 h in dependence of the O_2 concentration. Modified from [76] © 2023.

derived Pt(IV) prodrugs with axial ligands conjugated with naphthalimide derivatives [77,78]. The amino-derivative **O-2a** and unsubstituted **O-2b** were cytotoxic in a panel of cell lines with results comparable to those for cisplatin and oxaliplatin, apart from slightly higher activity in the cisplatin-resistant variant A549R. Moreover, *in vivo* a slightly reduced tumour weight was observed in CT26 xenograft tumours in BALB/c mice for **O-2a** relative to oxaliplatin treatment (83 *vs.* 62%), while the tumour volume was similar to that observed with oxaliplatin for both compounds (Fig. 13). The reduced forms, *i.e.*, the Pt(II) equivalents of **O-2a** and **O-2b**, prepared through treatment with ascorbic acid, were more effective at damaging plasmid DNA than either oxaliplatin or the complexes without reductant present, which supports a synergistic effect from the components and reduction-induced activity. For **O-2b**–**O-2e** minor variation in the activity was observed in the cell line panel.

The same naphthalimide ligands used in **O-2a**–**O-2e** were also utilised to form the bisnaphthalimide Pt(IV) analogues of oxaliplatin and cisplatin **O-3a**–**O-3e** and **O-4a**–**O-4e** (Fig. 14) [79,80]. Of the oxaliplatin prodrugs **O-3a**–**O-3e**, only **O-3c** showed comparable activity to **O-1a**, which was attributed in part to the poor water solubility of the bisnaphthalimide compounds, as well as apoptosis induction [79]. The anticancer activity appears to be due to DNA interaction of the compounds as confirmed by spectroscopic studies and DNA platination studies in cells. The cisplatin derivatives **O-4a**–**O-4e** mirror the properties of the oxaliplatin analogues. The amino-derivative **O-4a** was the most cytotoxic, although **O-4c** did show comparable activity in the cancer cell lines SKOV-3, A549R and HeLa [80]. This could be related to the balance of water solubility and lipophilicity which is an important consideration that can have large effects on the cytotoxicity of anticancer agents, due to the effect on cellular uptake and accumulation

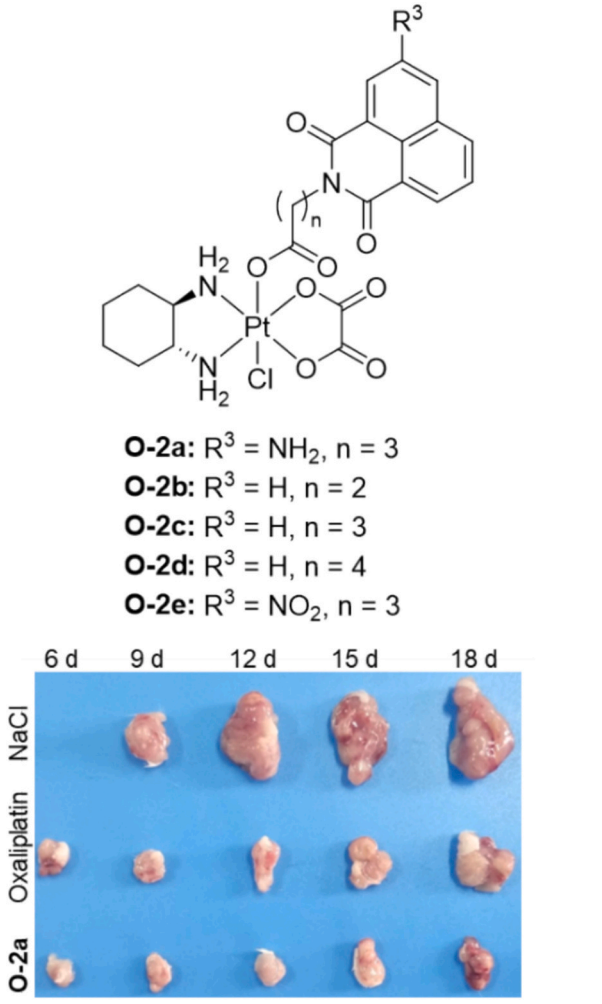

Fig. 13. Chemical structure and *in vivo* antitumour activity studies of **O-2a** compared to oxaliplatin and NaCl. Modified from [77] with permission from Elsevier © 2019.

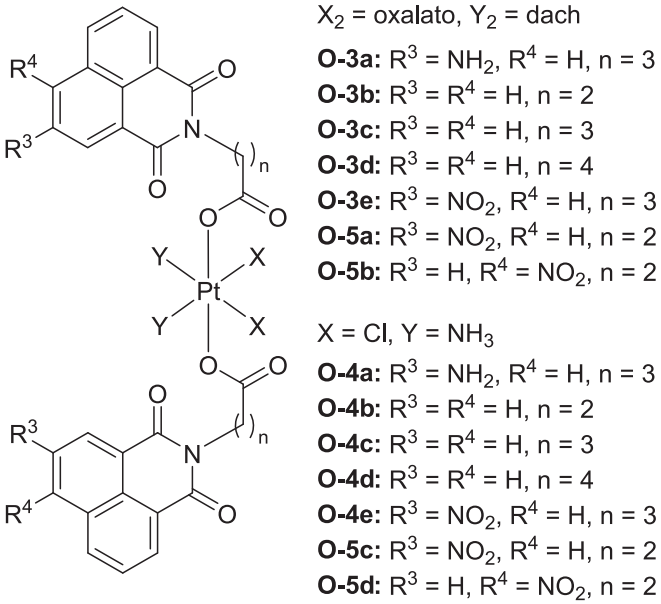

Fig. 14. Pt(IV) prodrugs for cisplatin and oxaliplatin [dach = (*1R,2R*)-diaminocyclohexane] with dual naphthalimide-based axial ligands.

[81].

A series of nitro-derivatives **O-5a**–**O-5d** (Fig. 14) were also developed in which the position of the nitro substituent on the two naphthalimide prodrugs was varied. The cisplatin prodrug **O-5d** showed the highest activity in all cancer cell lines tested, with higher potency than either cisplatin or oxaliplatin alone. This was pronounced in the chemoresistant cell lines MDA-MB-231, 4T1, and A549cisR [57], indicating that the naphthalimide ligand may be exerting a synergistic function which augments the activity of cisplatin and oxaliplatin. **O-5b** and **O-5d** both showed higher activity than their counterparts with R^3-substituted nitro groups, which could be an indication that substitution at the R^4 position may be most favourable for higher cytotoxicity for nitro-naphthalimide derivatives.

The *trans*-azido complexes **O-6a**–**O-6c** (Fig. 15) were designed to intercalate DNA and upon photoactivation produce ROS and platinate DNA after reduction to the respective Pt(II) species [82]. **O-6a** was shown to bind to DNA by linear dichroism spectroscopy, with viscometry suggesting the length of DNA increased upon binding. While **O-6b** was fluorescent and bound to DNA, the latter was much weaker than found for **O-6a**, while **O-6c** did not show any detectable DNA binding. This suggests that larger steric bulk of naphthalimide substituents is detrimental to DNA binding. However, **O-6a** also possessed poor aqueous solubility, limiting further photocytotoxicity studies. Despite the lesser DNA-binding affinity of **O-6c**, it showed comparable photocytotoxicity to **O-6b** after incubation and irradiation at 465 nm and could also be activated by light at 520 nm.

The Pt(IV) complexes **N-6a**–**N-6d** (Fig. 15) are prodrugs of the Pt(II) compounds **N-6a**–**N-6d** [58]. They were found to be more stable in DMSO than the Pt(II) analogues. In gel electrophoresis experiments with plasmid pBR322, none of the Pt(IV) complexes alone interacted with DNA. Significant changes were seen upon incubation with either of the biological reductants ascorbic acid or glutathione, with the most significant results seen for **N-6c** and **N-6d**. However, despite the greater interaction with DNA of the other complexes, **N-6a** and **N-6b** showed significantly greater cytotoxicity at a sub-μM level in A2780 cells (0.06 μM) compared to 2.5 and 1.7 μM for **N-6c** and **N-6d**, respectively. All complexes were significantly more cytotoxic than their Pt(II) counterparts, attributed to a higher logP value since higher lipophilicity also suggests higher cell uptake.

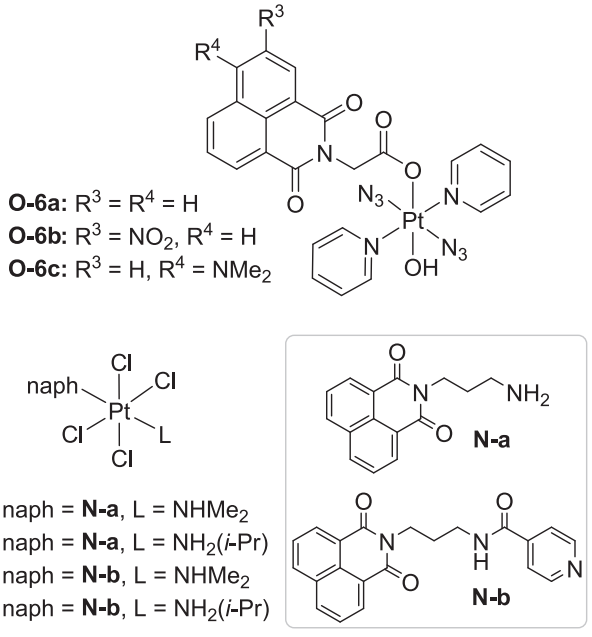

Fig. 15. Structures of the photoactivatable diazido complexes **O-6a**–**O-6c**, and the Pt(IV) prodrugs **N-6a**–**N-6d**.

Complexes **O-7a**–**O-7j** (Fig. 16) were designed as Pt(IV) prodrugs of oxaliplatin (**O-7a**–**O-7g**) or cisplatin (**O-7h**–**O-7j**) [83]. Functionalisation with naphthalimide was aimed to increase the cytotoxicity of the platinum pharmacophore through targeting specific mechanisms associated with the development of resistance. The naphthalimide Pt(IV) prodrugs of cisplatin (**O-7h**–**O-7j**) were found to inhibit cell growth across the cancer cell line panel, with similar or higher potencies compared to cisplatin and oxaliplatin, and **O-7i** identified as having the highest cytotoxicity overall. Among the oxaliplatin prodrugs, there was no clear trend in activity between those carrying one or two axial naphthalimide ligands, nor modification of the naphthalimide core.

Compound **O-7i** was demonstrated to show *in vivo* activity in C57BL/6 mice bearing glioblastoma with an inhibition level of 64.3% compared to cisplatin (26.7%) and temozolomide (40.3%) [83]. The complex was found to be more potent than a combination of cisplatin and the free ligand. The compound was well tolerated *in vivo* and the pharmacokinetic parameters demonstrated the applicability of the compound in a therapeutic setting. Its targeted activity against factors commonly implicated in cisplatin resistance of glioblastoma, namely increased lysosome abundance and recruitment of tumour-associated macrophages, was investigated. Lysosomes are able to sequester and degrade cisplatin, hence increased lysosome abundance can confer resistance to cisplatin as it fails to accumulate in the nucleus to a sufficient extent

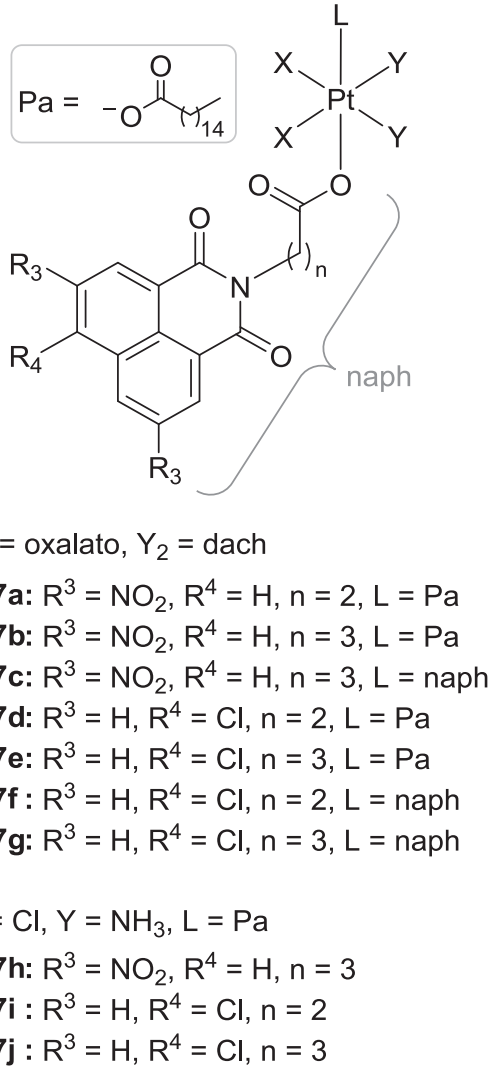

Fig. 16. Structures of the Pt(IV) prodrugs of oxaliplatin or cisplatin **O-7a**–**O-7j** (Pa = palmitate).

[84,85]. Treatment of two glioblastoma cell lines with **O-7i** was found to decrease not only the abundance of lysosomes but also the extent of Pt uptake by the remaining lysosomes, proposed to be due to the activity of the palmitate fatty acid component regulating lysosomal autophagy.

Tumour-associated macrophages are well understood for their role in promoting the tumour microenvironment and suppressing immune activation as M2 polarised macrophages, but the direct mechanisms by which they promote cisplatin resistance are yet unclear [86]. Regardless, **O-7i** was found to significantly reduce the number of M2 polarised macrophages in both *in vivo* and *in vitro* studies, which could be a contributing mechanism towards its observed cytotoxic activity and also reinforces its potential to inhibit or reverse treatment-associated cisplatin resistance [83].

3.2. Ruthenium complexes functionalised with naphthalimide

Just as the discovery of cisplatin led to the development of other Pt anticancer agents, it also steered interest towards investigation of complexes of other metal centres with anticancer activity. Changing from Pt to other metal centres has been hypothesised to circumvent the common acquired and intrinsic resistances to the Pt agents by various cancers [62,71,87]. Due to similar physicochemical properties of Pt(II) and Ru(II)/Ru(III) complexes, the latter have attracted early interest as an alternative to Pt. Furthermore, due to their propensity to undergo redox reactions and possibly mimic some properties of Fe, given the position in the Table of Elements, additional beneficial physiological properties were anticipated. Eventually, several Ru compounds entered clinical trials including TLD1433 (ruvidar®) as a photodynamic therapy (PDT) agent and cytotoxic BOLD-100, which are both currently undergoing clinical evaluation [88–91].

3.2.1. Polypyridyl-type complexes

Polypyridyl ligands are often paired with Ru centres for use as photosensitisers (PS) in PDT [92,93]. Gunnlaugsson and co-workers were the first to functionalise Ru(II) polypyridyl complexes with naphthalimide arms (**NN-2a**, **NN-2b**, **NN-3a**–**NN-3d**, **NN-4a**, **NN-4b**; Fig. 17) to increase the DNA binding affinity and light-harvesting efficiency, also observing DNA photocleavage [94–96]. The 1,4,5,8-tetraazaphenanthrene (TAP) complexes **NN-3a**–**NN-3d** showed the highest binding affinity to DNA which was attributed to the meta-arrangement resulting in a wedged compound that allowed closer association with DNA [95]. The amine derivatives showed stronger DNA binding affinity in various studies, however, the nitro derivative **NN-3a** produced more significant results in the DNA photocleavage experiments and was also not affected by the presence of a singlet oxygen scavenger. This indicates that the mechanism for these complexes is independent of singlet oxygen, unlike the PDT type II mechanism typically displayed by Ru(II) polypyridyl complexes [97]. The bipy complex **NN-3d** was found to show the highest photocytotoxicity despite its low DNA photocleavage efficiency [95]. This suggests that DNA photocleavage may not be the predominant mode of action for the photocytotoxicity but rather photoinduced ROS generation. This is based on the activity of these compounds being quenched in the presence of a singlet oxygen scavenger and enhanced in D_2O, which prolongs the lifetime of ROS to produce more damage.

NN-4a and **NN-4b** (Fig. 17) were designed as dual imaging and therapeutic agents, with the naphthalimide moiety intended to aid cell uptake and DNA-binding [96]. For the bisnaphthalimide derivative **NN-4b**, the DNA binding affinity increased while the photocleavage efficiency decreased, inferred to be due to the additional naphthalimide-DNA interaction hindering close association between the Ru-polypyridyl centre and DNA. The intensity of the metal to ligand charge transfer (MLCT) emission in the presence of DNA after excitation at 338 nm was decreased by ~43% while the naphthalimide-centred emission was not affected, supporting its potential use as a DNA imaging agent. Upon light activation, significant DNA cleavage was seen, and the IC_{50} value in HeLa was reported as 7.81 μM compared to almost 30 μM in the dark. The Ru(II) polypyridyl complexes **NN-5a** and **NN-5b** (Fig. 18) were designed to resemble traditional organic naphthalimide agents and were shown to retain significant levels of TOP2α inhibition and extended the inhibitory activity towards TOP1 [98]. Binding through intercalation, their DNA-binding affinity was several magnitudes greater than found for $[Ru(bipy)_3]^{2+}$ (bipy = 2,2′-bipyridine) and $[Ru(phen)_3]^{2+}$ (phen = 1,10-phenanthroline) and comparable to that of the established DNA intercalator ethidium bromide (EtBr). However, viscosity titrations and thermal denaturation studies suggested that they did not disrupt the DNA structure as much as EtBr, although the greater lipophilicity of the ancillary ligands of **NN-5a** gave a slightly higher binding affinity. Photocleavage of plasmid DNA to the open circular

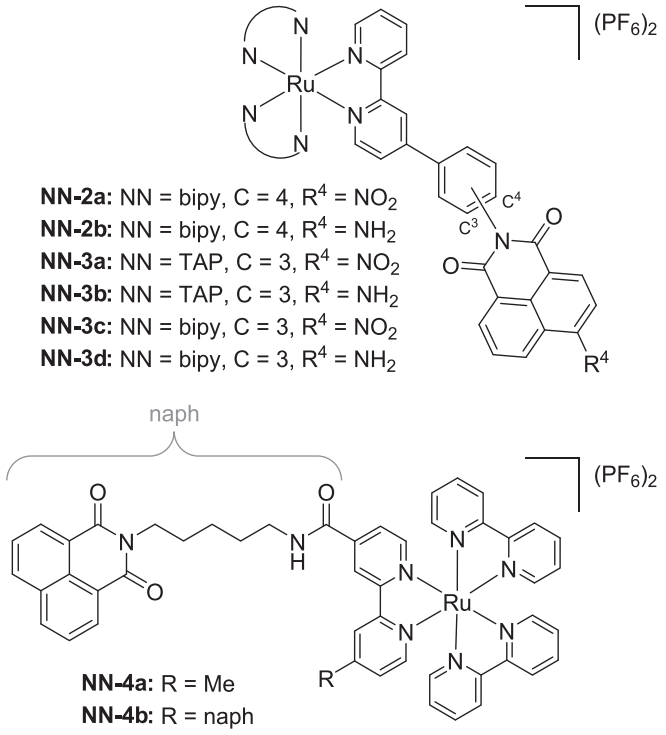

Fig. 17. Chemical structures of Ru(II) polypyridyl complexes **NN-2a**, **NN-2b**, **NN-3a**–**NN-3d**, **NN-4a**, and **NN-4b**.

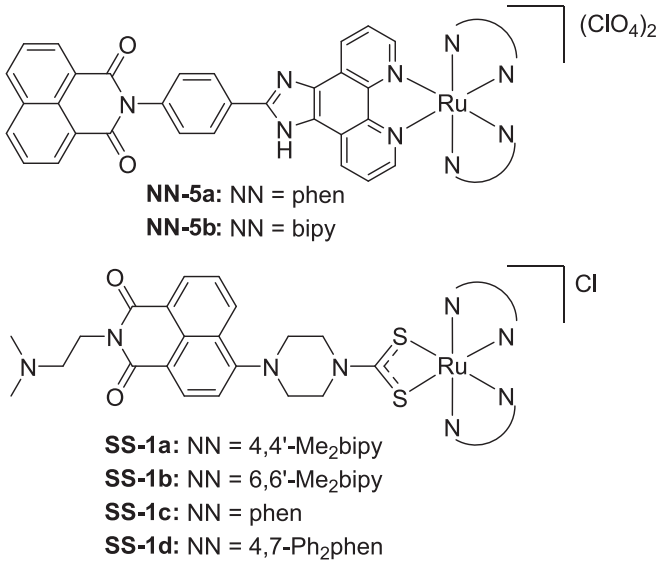

Fig. 18. Chemical structures of Ru(II) imidazophenanthroline complexes **NN-5a** and **NN-5b**, and of dithiocarbamato complexes ***SS*-1a**–***SS*-1d**.

form was seen at 15 μM, and IC_{50} values of approximately 4.5 and 4.0 μM were estimated for TOP1 and TOP2α, respectively. **NN-5a** was also shown to bind to and stabilise RNA triplexes [99], having positive implications for potential cytotoxic or cytostatic activity, although this has yet to be investigated.

The polypyridyl complexes **SS-1a**–**SS-1d** (Fig. 18; Tables 1 and S8) pair the bioactive moieties of a Ru(dithiocarbamato) moiety and an amonafide-like naphthalimide [100]. All complexes showed moderate to good cytotoxicity against cancer cells, with **SS-1a** generally being the most potent at low-μM cytotoxicity in A549 cells, which was retained in the cisplatin-resistant variant (A549cisR). Guided by proteomics data, a range of mechanistic investigations were carried out which suggested **SS-1a** could exert the cytotoxic activity through multiple pathways, predominantly involving mitochondrial damage such as reducing MMP, damaging inner membrane cristae, and reducing metabolic function. It may also function to stimulate an immune response, suggested initially by proteomics and consequently through *in vivo* experiments, in which the splenocyte population in mice treated with **SS-1a** had a significantly increased proportion of CD4 and CD8 T lymphocytes. Unlike the other polypyridyl complexes, the photophysical properties of the dithiocarbamato complexes were not investigated.

Gunnlaugsson et al. prepared the water-soluble Ru(II) polypyridyl complexes **NN-6a** and **NN-6b** (Fig. 19) bearing two naphthalimide moieties conjugated *via* Tröger's base with bipyridyl coordinating moieties [110,111]. Originally investigated as cellular probes, the DNA binding capability of the two compounds was investigated. In spectroscopic titrations with salmon testes DNA (stDNA), no significant deviations were observed in absorption or emission spectra. However, both compounds shifted the melting transition (T_m) of stDNA significantly, with **NN-6a** producing the greatest shift from an initial T_m of 69 to over 85 °C (10 mM phosphate buffer, 50 mM NaCl), with melting still incomplete at 90 °C. Both compounds showed complete uptake in HeLa cells after 4 h, with the red emission of the compounds visible in the cytoplasm as well as in and around the nucleus.

Although initial studies revealed no cytotoxicity towards HeLa cells over a range of concentrations, **NN-6a** was found to induce membrane blebbing and **NN-6a** together with **NN-6b** was later investigated further for use in PDT [111]. In these subsequent experiments, the uptake of the compounds into peripheral blood mononuclear cells (PBMC) obtained from healthy individuals was found to be significantly lower than in HeLa cells. In the cancer cells, endocytosis was found to be the predominant cellular uptake mechanism, which for **NN-6a** was caveolae- and lipid raft-dependent. Although it was initially reported that the compounds were found partially in and around the nucleus, experiments following the determination of the cellular uptake mechanism revealed that the compounds predominantly accumulated in the Golgi complex and lysosomes (Fig. 19), with a more modest accumulation also in mitochondria. Both compounds displayed no cytotoxicity in the dark against HeLa cells but a 1 h photoactivation period followed by 23 h incubation resulted in significant cytotoxicity and gave IC_{50} values of 1.8 ± 0.3 μM and 4.6 ± 0.7 μM for **NN-6a** and **NN-6b**, respectively, through induction of late-stage apoptosis. Cell shrinkage and significant disruption to tubulin structure were observed after treatment with both compounds, although they were more pronounced for **NN-6a**. ROS production also occurred, particularly in mitochondria, in which the compounds induced rapid changes in morphology after light activation. Given the compounds were not significantly localised in nuclei and accordingly DNA binding and damage would be limited, the light-dependent cytotoxicity was noted as highly promising and suggest these compounds may be suitable for use in PDT.

3.2.2. *Piano-stool complexes*

In addition to their use in Ru(polypyridyl) complexes, naphthalimide moieties have been attached to various Ru(II)-arene piano-stool complexes. These complexes are easily modifiable and the framework lends itself to the design of multifunctional agents [71,87]. Incorporating a naphthalimide moiety in Ru(II) piano-stool complexes can be performed either through conjugation to the π-bound arene or functionalisation of an ancillary ligand [6,101].

3.2.2.1. Piano-stool complexes of N-donor ancillary naphthalimide-functionalised ligands. By functionalisation of an *N*-donor ancillary ligand with naphthalimide moieties, **N-7a**–**N-7d** and **N-8a**–**N-8c** (Fig. 20) were reported [101,112]. Compounds **N-7a**–**N-7d** were more cytotoxic in comparison to RAPTA-C, and the derivatives with unsubstituted naphthalimides, *i.e.*, **N-7b** and **N-7d**, were less cytotoxic than the dimethylamine derivatives **N-7a** and **N-7c**. The increase in cytotoxicity for the complexes with a dimethylamine-substituted naphthalimide suggests DNA intercalation is involved in the mechanism of action since small nitrogen substituents at this site have been reported to increase cytotoxicity through increased DNA-binding affinity [50]. The reported IC_{50} values for **N-7c** of 6.5 μM in A2780 and 8.6 μM in A2780R indicate a similar level of cytotoxicity in the chemoresistant variant. **N-8a**–**N-8c** (Fig. 20) feature a bipy ligand and are thus more alike the

Table 1
IC_{50} values (μM) determined in cancer cell lines with the MTT assay for lead compounds in series of cytotoxic piano-stool and NHC metal complexes modified with naphthalimide, as well as auranofin-like derivatives. The IC_{50} values are given in those cell lines in which the test compounds exhibited the highest activity and most commonly cisplatin was used as the control compound.

Compound	Cancer cell line	IC_{50} / μM	IC_{50} / μM control compound	IC_{50} / μM ligand	Treatment time / h	Ref.
SS-1a	A549	4.13 ± 0.69	15.89 ± 0.24	>50	48	[100]
N-7a [1]	A2780	6.1 ± 1.1	230	18.5 ± 0.3	72	[101]
Ar-1b [1]		2.31 ± 0.1		–		
N-10a [2]	HeLa	2.0 ± 0.3	13	>100	48	[102]
NN-7b	CRL7687	1.103 ± 0.8	19.7 ± 2.0 [3]	0.620 ± 0.1	72	[60]
NO-1a		0.724 ± 0.3	0.627 ± 0.4 [3]	0.724 ± 0.2		
NHC-1 h	MCF-7	1.7 ± 0.2	–	0.6 ± 0.02	72	[103]
NHC-2e		1.7 ± 0.3		1.9 ± 0.4		[104]
NHC-3a		0.2 ± 0.02		0.2 ± 0.01		[103]
NHC-4c		2.0 ± 0.2		5.2 ± 0.6		[105]
NHC-5d		2.1 ± 0.5		4.6 ± 3.6		[106]
NHC-6 h	MCF-7	4.82 ± 0.77	–	33.23 ± 5.84	96	[107]
NHC-7 [4]	A549	0.059 ± 0.003	2.23 ± 0.12	0.134 ± 0.025	72	[108]
S-1c	MCF-7	1.1 ± 0.1	–	3.1 ± 0.4	72	[109]

[1] RAPTA-C used as the control compound.
[2] IC_{50} values determined with the alamarBlue assay.
[3] As no control compound was tested, instead the IC_{50} value presented is of the compound in the healthy cell model CA-M75.
[4] Test compounds pre-incubated with 6 eq. bovine serum albumin (BSA). As the naph ligand was not tested, instead the IC_{50} value presented is of the metal complex lacking the naph component.

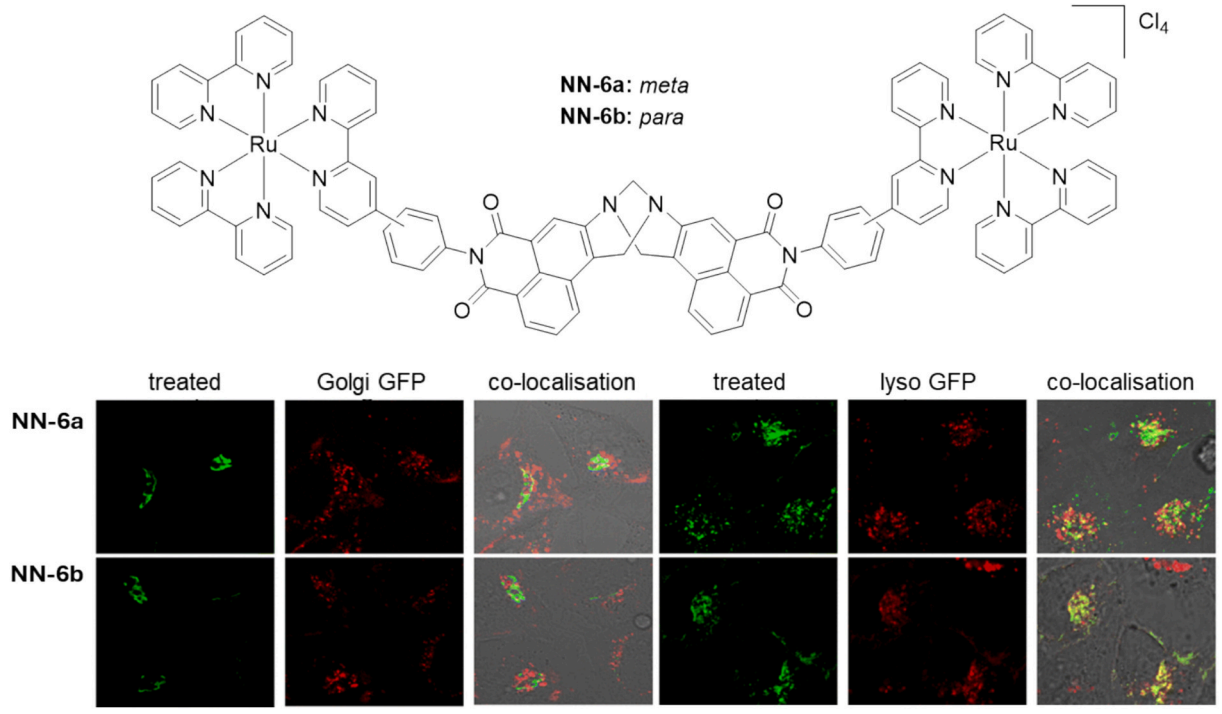

Fig. 19. (Top) Structure of dimetallic Ru(II) polypyridyl naphthalimide complexes **NN-6a** and **NN-6b** conjugated *via* Tröger's base. (Bottom) Confocal microscopy showing compounds in HeLa cells localising in Golgi apparatus, lysosomes, and mitochondria when stained with DAPI and co-stain GFP (green fluorescent protein), and the effects of compounds on α-tubulin and actin. Modified from [111] © 2024.

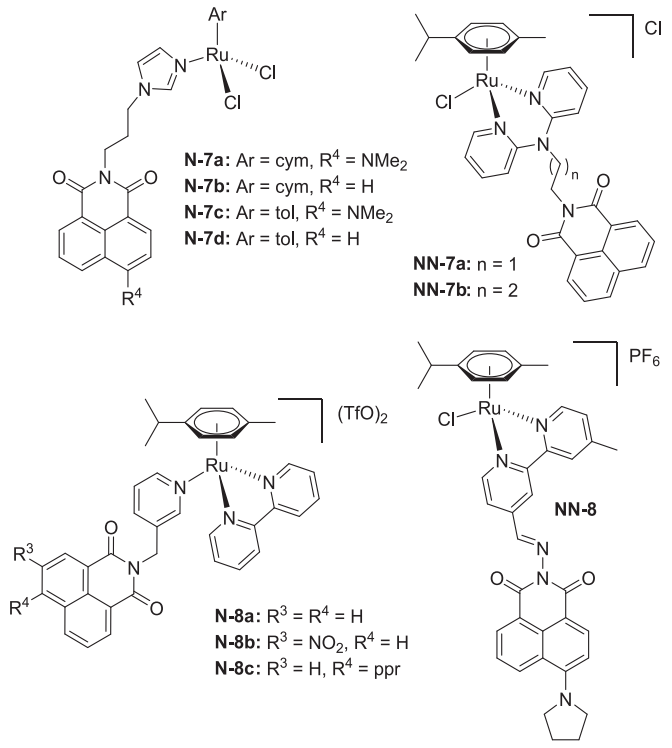

Fig. 20. Ru(II) anticancer agents with R^N-naphthalimide-substituted ancillary ligands (cym = η^6-*p*-cymene, tol = η^6-toluene, ppr = piperidine).

polypyridyl compounds (*vide supra*) in that they are intended to be photoactivated, specifically for use in photoactivated chemotherapy (PACT) [112]. Designed to release the naphthalimide ligand upon irradiation, only **N-8c** underwent complete photolysis after 3 h of radiation while over 50% of **N-8a** and **N-8b** were still intact. Concordant with these results, the only compound to show significant cytotoxicity in A549 cells was **N-8c** (IC_{50} 10.5 μM) after 24 h of incubation with the drug followed by irradiation for 3 h at 420 nm.

NN-7a, **NN-7b**, and **NN-8** (Fig. 20) feature a naphthalimide conjugated to a bidentate-coordinating bi- or di-pyridyl moiety, with the ligand of **NN-8** also found in a series of Ir(I) compounds (**NN-11a**–**NN-11c**, *vide infra*). **NN-8** showed no cytotoxicity towards the cancer models tested (A549, HeLa, HepG2) [113] although photocytotoxicity was not investigated. Compounds **NN-7a** and **NN-7b** and the Schiff base complexes **NO-1a**–**NO-1c** (Fig. 21) exhibited cytotoxicity in CRL7687 melanoma cells at sub-μM concentrations but were also similarly active in the healthy melanocyte cell model CA-M75 [60]. **NN-7b** showed high cytotoxicity towards CRL7687 cells with an IC_{50} value of 1.1 μM, while it gave an IC_{50} value of 20 μM in the healthy cell model.

N-9a and **N-9b** (Fig. 21) are both water-soluble compounds with $\log P_{o/w}$ values of −0.05 and − 0.71, respectively, indicating mild hydrophilicity which is likely due to the morpholine substituent [114]. This is in contrast to most other naphthalimide anticancer agents which are lipophilic and thus typically have more efficient cell uptake. However, particularly for **N-9a**, cell uptake was sufficient to visualise its green luminescence within cells, where it was found to localise mostly in nuclei and lysosomes. The lysosome localisation was attributed to the morpholine moiety rather than the naphthalimide, with the overall localisation supporting the ability of these compounds to exhibit dual modes of action from different moieties within the same metal complex. Designed as PS for PDT or PACT, **N-9a** and **N-9b** were more cytotoxic than cisplatin in MCF-7, A498 and HeLa cancer cells upon light irradiation, while showing less or similar cytotoxicity to cisplatin in the healthy cell models NRK and NIH.

The dimetallic piano-stool complexes **N-10a** and **N-10b** (Fig. 22) feature two naphthalimide moieties conjugated *via* Tröger's base and carry curcumin as ancillary ligands [102,115]. The naphthalimide component is highly emissive due to the intramolecular charge transfer-based transitions and wedged structure, while the curcumin moiety has

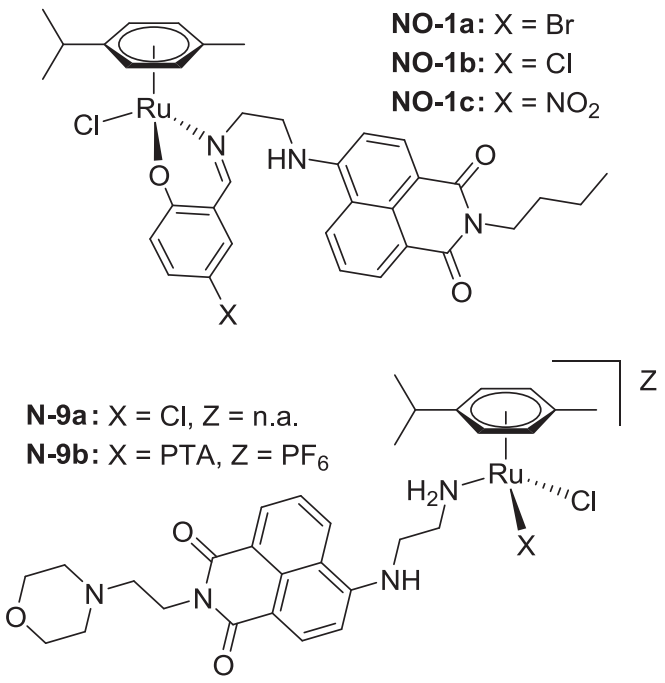

Fig. 21. Schiff base complexes **NO-1a**–**NO-1c** and photocytotoxic **N-9a** and **N-9b** (PTA = 1,3,5-triaza-7-phosphaadamantane).

been demonstrated to have a range of beneficial bioactivities on its own [116,117] and when conjugated to Ru(II) piano-stool compounds [118,119]. The emission of the naphthalimide moiety within the Ru complexes was largely quenched compared to the free ligand, which was suggested to be due to energy transfer between the naphthalimide excited state to curcumin and overlap of the emission band with the MLCT absorption. However, both compounds were significantly more cytotoxic than cisplatin in cancer cells with IC_{50} values in the low μM range. Interestingly for **N-10a**, the free naphthalimide ligand also showed moderate cytotoxicity with an IC_{50} value of 25 μM, while the ligand in **N-10b** with the extended spacer between the naphthalimide moiety and the coordinating pyridyl group was non-cytotoxic.

Compounds, **N-11a**–**N-11c** (Fig. 22) are structurally related to **N-10a** and **N-10b** with the most significant distinction in this new series being the replacement of the curcumin ligand with two exchangeable chlorido ligands [120]. Designed predominantly as fluorescent bioimaging probes, **N-11a** and **N-11b** showed good cell uptake and low cytotoxicity in 3T3 mouse embryonic fibroblast cells, in addition to relatively strong binding to BSA [121]. **N-11c** was not extensively investigated as it was observed to have poor cell uptake and formed aggregates at the cell membrane border [120]. The non-cytotoxicity of **N-11a** and **N-11b** is in stark contrast to the significant cytotoxicity observed for **N-10a** and **N-10b**, indicating that the curcumin co-ligand is important for their cytotoxicity. This can be considered analogous to the core design principle for organic naphthalimide anticancer agents, wherein the intrinsic DNA binding activity of the naphthalimide only translates to cytotoxic activity upon substitution of the core naphthalimide scaffold to introduce a complimentary mechanism. Compounds **N-11a** and **N-11b** are structurally related to cytotoxic **N-7a** and **N-7c**. The dimeric nature of **N-11a** and **N-11b** may render them more sterically demanding, possibly limiting their interaction with DNA or proteins at the exchangeable chlorido ligand sites.

3.2.2.2. From N-donor to C-donor ligands. The piano-stool complex **CN-1a** and the structurally related trithiacyclononane complexes **CN-1b**–**CN-1d** (Fig. 23) were developed as protein kinase inhibitors, with **CN-1b** investigated more in depth [122]. Kinase inhibitors have been widely investigated for the treatment of cancer and often they feature large, planar aromatic structures to, for example, block the ATP-binding sites on the proteins [123]. Of the 442 enzymes tested, there were 8 protein kinases distributed among four families for which the compound exhibited very strong inhibition. For MYLK, which is involved in regulating smooth muscle contraction, **CN-1b** was a very strong inhibitor with an IC_{50} value of 75 ± 20 nM, while the naphthalimide ligand alone displayed no inhibitory activity. Despite the high inhibition of MYLK by **CN-1b**, *in vitro* cytotoxicity studies found that it did not significantly inhibit the proliferation of either 451Lu or WM3918 melanoma cells. However, **CN-1a** showed marked cytotoxicity in 451Lu and WM3918 cancer cells with IC_{50} values up to 20 μM, while it was substantially less cytotoxic towards the healthy cell models FOM102010 and FF2508.

Besides *N*-donor ligands, naphthalimides have also been tethered to *N*-heterocyclic carbenes (NHCs) as coordinating moieties (Tables 1 and S7). Metal(NHC) complexes are generally very stable in biological environments, making NHCs ideal anchor ligands for the naphthalimide DNA-targeting and -intercalating moiety [103,105]. Several series of naphthalimide-NHC complexes with Ru(II) (**NHC-1a**–**NHC-1h**), as well as Rh(I) (**NHC-2a**–**NHC-2h**), and Ag(I) (**NHC-3a**–**NHC-3b**) (Fig. 24)

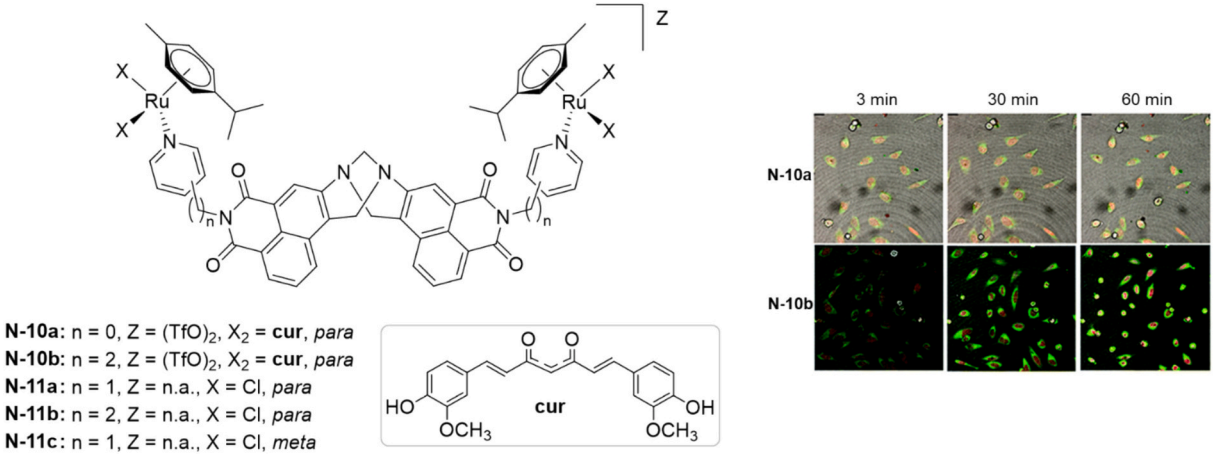

Fig. 22. (Left) Chemical structures of the dimetallic piano-stool Ru(II) naphthalimide complexes conjugated *via* Tröger's base, **N-10a** and **N-10b**, and **N-11a**–**N-11c**. (Right) Confocal live images of **N-10a** and **N-10b** (5 μM) within HeLa cells after various periods of incubation, with green fluorescence from the metal complex and red fluorescence from DRAQ5 nuclear stain. Modified from references [102,115] with permission of the American Chemical Society ©2022 and the Royal Society of Chemistry ©2018 https://doi.org/10.1039/C8CC01584H, respectively. (For interpretation of the references to colour in this figure legend, the reader is referred to the web version of this article.)

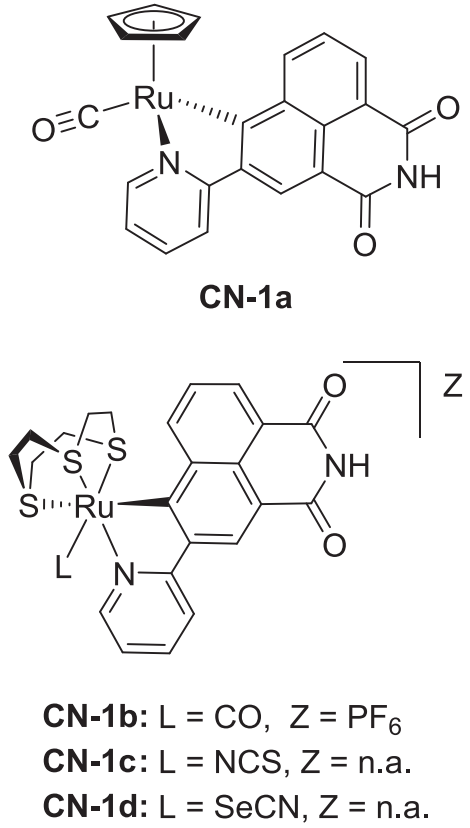

Fig. 23. Chemical structures of the Cp complex **CN-1a** and its trithiacyclononane analogues **CN-1b**–**CN-1d**.

were developed with mono- or bis-naphthalimide substitution. Coordination to metal centres mostly resulted in quenching of fluorescence, with the exception of **NHC-1f** and **NHC-2f** bearing electron-rich thio-substituents on the naphthalimide and benzyl-substituents on the NHC [104]. Substitution of the naphthalimide-NHC with a secondary lipophilic group was associated with improved cytotoxicity, likely due to increased cellular accumulation and retention. For organometallics bearing unsubstituted mononaphthalimide ligands (**C-2a**–**C-2i**), cytotoxicity increased in the order Ru(II) < Rh(I) < Cu(I) in MCF-7 and HT-29 cells. The thioether compounds all showed lower or equal cytotoxicity to the pro-carbene compounds in MCF-7. In HT-29 cells some complexes showed improved potency over the respective pro-carbenes, with **NHC-1f** being the most cytotoxic with an IC_{50} value of 4.9 μM, compared to 9.6 μM for the pro-carbene [104]. Among the bis-naphthalimide-functionalised complexes, only the Ag(I) compounds **NHC-3a** and **NHC-3b** gave similar cytotoxicity to the pro-carbenes, while **NHC-3a** was slightly more cytotoxic overall [103].

In further investigations into the activity and modes of action of **NHC-1f** and **NHC-2f** and the free naphthalimide-NHC ligand in HCT116, MCF-7 and MDA-MB-231 cancer cell lines, both metal complexes showed increased cytotoxicity in HCT116 compared to the free ligand, contrasting the inverse relationship in MCF-7 [124]. **NHC-1f** was found inferior to both **NHC-2f** and the pro-carbene in inhibiting cell cycle progression and to the pro-carbene in producing ROS. While **NHC-1f** was inferior to the ligand in producing cellular ROS, it was more active in inducing mitochondrial ROS at all timepoints. It was found to exert this effect through increasing the mitochondrial membrane potential (MMP) and thus sensitising the membrane to apoptogenic factors. Production of mitochondrial ROS is associated with activation of the p38 mitogen-activated protein kinase (MAPK) pathway, which leads to pro-apoptotic signalling. **NHC-1f** and **NHC-2f** were found to also induce p38 MAPK in MCF-7 and MDA-MB-231 cells, although to a lesser extent in the latter.

The same compounds were subjected to antimicrobial studies and they were overall significantly more active in inhibiting the growth of gram-positive bacteria compared to gram-negative bacteria or fungi [104]. Overall, **NHC-1f** and **NHC-2f** were the most active inhibitors of gram-positive bacterial growth, with **NHC-1f** exhibiting MIC values of 8 μg/mL, while **NHC-2f** was less active in the *B. subtilis* strain tested but reached an MIC of 4 μg/mL in a *Staphylococcus aureus* (*S. aureus*) strain.

3.2.3. 3.2.2.3 π-bound ligands functionalised with naphthalimide moieties

Based on the RAPTA-C scaffold, **Ar-1a**–**Ar-1c** (Fig. 25) feature a naphthalimide conjugated to the π-bound benzene group rather than at the more readily exchangeable ligand coordination sites [101]. Complexes like RAPTA are often highly water soluble due to the presence of the amphiphilic PTA ligand [71,125], with **Ar-1a**–**Ar-1c** soluble in water

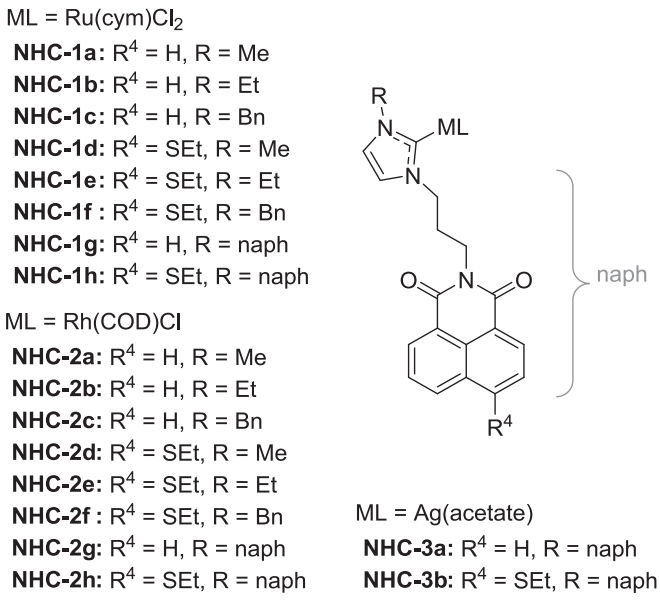

Fig. 24. Structures of NHC complexes of Ru(II) **NHC-1a–NHC-1h**, Rh(I)-cyclooctadiene (COD) **NHC-2a–NHC-2h**, as well as of Ag(I)-acetate **NHC-3a** and **NHC-3b**.

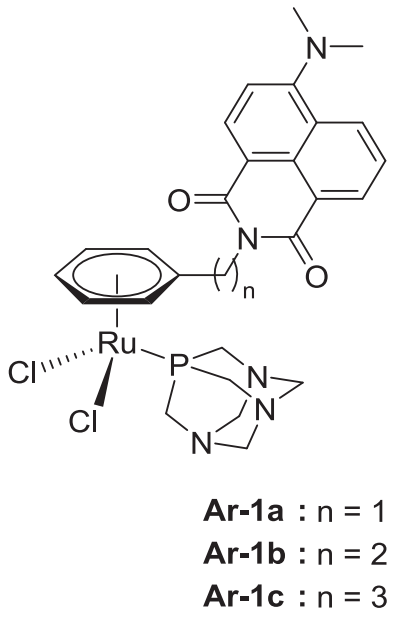

Fig. 25. Arene-conjugated RAPTA-derived compounds **Ar-1a–Ar-1c**.

and undergoing rapid aquation within 30 min to the monoaqua species, although not proceeding spontaneously to the doubly aquated species. All complexes were significantly more cytotoxic than RAPTA-C in the cancer cells tested, with **Ar-1b** showing the highest cytotoxicity in A2780 cells and the resistant variant A2780R with IC_{50} values of 2.3 μM. While guanosine binding studies suggested **Ar-1b** showed less affinity for coordination to DNA than RAPTA-C, UV–vis and circular dichroism spectroscopy studies indicated that it significantly bound to and disrupted the structure of ctDNA.

3.3. First-row d block metal anticancer complexes with naphthalimide-derived ligands

3.3.1. Cu complexes and derivatives

In addition to the Pt and Ru complexes modified with naphthalimide which have been investigated for biological properties, many complexes with first row transition metal centres have been reported and investigated [126]. In contrast to several of the Ru(II) complexes, for which fluorescence emission was quenched compared to the ligands, the Cu(I) complexes **NN-9a**–**NN-9c** (Fig. 26; Table S12) were slightly more emissive than their ligands, which was enhanced in aqueous over organic solvents [127]. Moderate DNA binding affinity was reported for **NN-9a**. The IC_{50} values reported in MCF-7 and A549 cells suggest non-cytotoxicity, however, cisplatin was also not active under the conditions studied. Similarly, the Cu(II) complexes **N-12a** and **N-12b** (Fig. 26) [128], and **N-13a** and **N-13b** (Fig. 27) [129] were seemingly inactive in cancer cells. Both series exhibited the same increase in fluorescence in aqueous solvents as the Cu(I) complexes, although no comparison was made to the fluorescence of the free ligands. Both compound series were reported to bind to BSA. Despite their non-cytotoxicity in the cancer cells tested, **N-13a** and **N-13b** induced plasmid DNA cleavage after irradiation at 365 nm, with the mechanism of action differing between the two complexes as DNA photocleavage from **N-13a** was quenched by

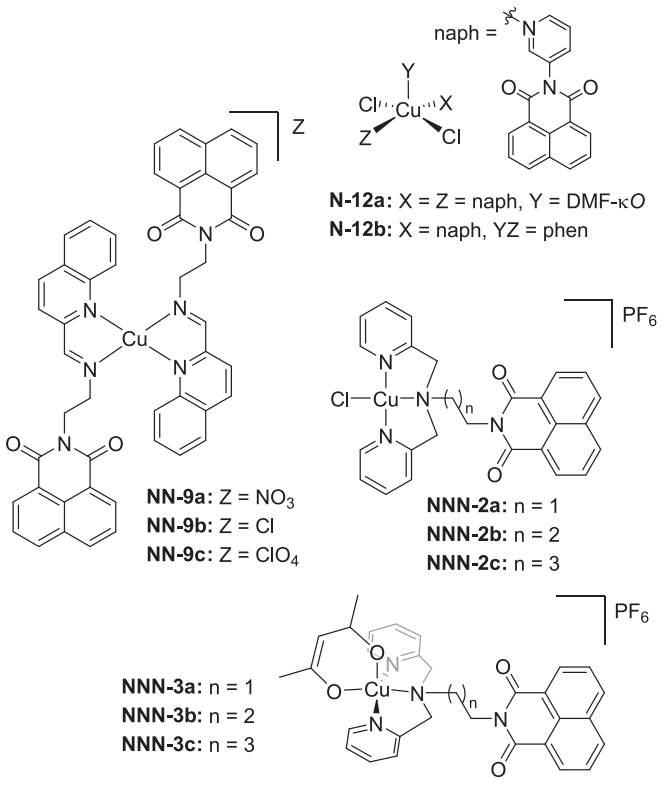

Fig. 26. Structures of Cu(I) complexes **NN-9a**–**NN-9c** and the related square pyramidal Cu(II) complexes **N-12a** and **N-12b**, and complexes with tridentate naphthalimide-functionalised ligands **NNN-2a**–**NNN-2c** and **NNN-3a**–**NNN-3c**.

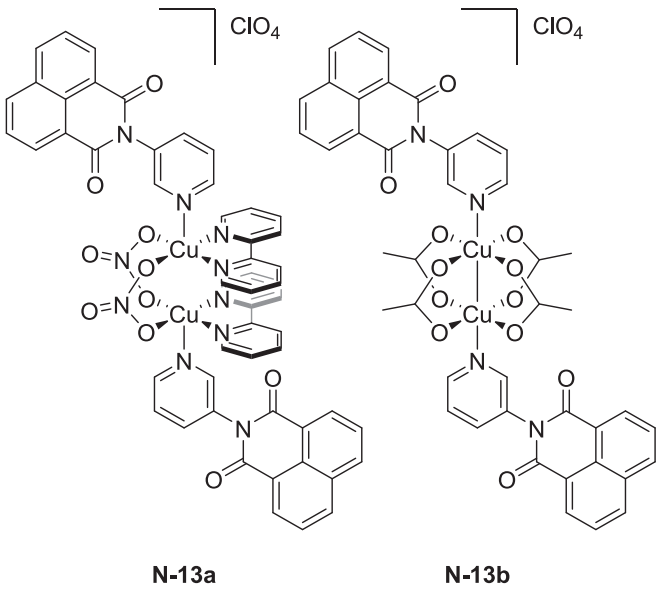

Fig. 27. Structures of di-Cu(II) complexes **N-13a** and **N-13b**.

ROS scavengers while for **N-13b** it was unaffected.

Cu(II) compounds **NNN-2a**–**NNN-2c** and **NNN-3a**–**NNN-3c** (Fig. 26) feature similar tridentate naphthalimide-functionalised ligands but differ in their co-ligands and thus also the geometry about the Cu(II) centre [130,131]. The compounds showed similar cytotoxicity despite the structural differences, probably due to weak interaction of the Cu centre with one of the coordinated acetylacetonato *O* donor atoms. In terms of biological activity, compounds with longer aliphatic linkers showed higher cytotoxicity, and **NNN-2c** and **NNN-3c** were similarly active in cancer cells and equal or superior to cisplatin. The Cu(II) complex lacking the naphthalimide substituent was moderately cytotoxic with IC_{50} values of approximately 40 μM, and significantly less cytotoxic than **NNN-2c** (IC_{50} values ≤10 μM), demonstrating the contribution of the naphthalimide fragment to the activity. **NNN-2c** and **NNN-3c** were found to intercalate into DNA with similar affinity.

NHC-4a–**NHC-4c** (Fig. 28) are the Cu(I) equivalents of the Ru(II) and Rh(I) complexes **NHC-1a**–**NHC-1c** and **NHC-2a**–**NHC-2c** (*vide supra*), of which **NHC-4c** was the only compound which was more cytotoxic than the naphthalimide pro-carbene [105]. Across the entire series of Ru, Rh, Ag, and Cu organometallics, the complexes containing naphthalimide-functionalised benzylimidazolylidene ligands were the most cytotoxic; hence, it was inferred that the role of the metal centre in the observed biological activity was minimal. Despite their promising cytotoxicity, the Cu compounds were found to be insufficiently stable for further studies.

ONO-1 (Fig. 29) is a Cu(II) complex with a rhodamine B-tagged

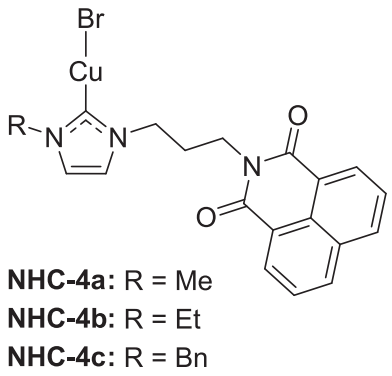

Fig. 28. Structures of Cu(I) complexes **NHC-4a**–**NHC-4c**.

naphthalimide ligand which undergoes a significant colour change from colourless to pink upon coordination to Cu(II), as the spirolactam ring of the free ligand opens upon coordination and extends the aromatic system across the rhodamine B component [132]. The complex was sensitive to the presence of sulfide and partially sensitive to azide, in the presence of which it reverted to the colourless free ligand but was resistant to other anions including some commonly present in biological systems such as chloride and dihydrogen phosphate. **ONO-1** was evaluated for its antiproliferative activity in cervical cancer cell lines HeLa and SiHa and in non-cancerous HEK293 cells. The complex was relatively nontoxic in HEK293 cells, while in HeLa and SiHa they were moderately active. In HeLa cells, fluorescence microscopy after staining with 2′,7′-dichlorodihydrofluorescein diacetate (H_2DCFDA) after exposure to **ONO-1** at the IC_{50} dose revealed a significant increase in ROS generation (Fig. 29). Staining with 4′,6-diamidino-2-phenylindole (DAPI) indicated significant chromatin condensation, and analysis of DNA extracted from the **ONO-1**-treated cells showed extensive fragmentation.

The Co(II), Cu(II) and Zn(II) complexes **Tpd-1a**–**Tpd-1c** with a tripodal, tridentate ligand (Fig. 30; Table S13) caused photoinduced DNA and protein cleavage [133]. The complexes showed similar DNA affinity, however, the degree of photoinducible DNA cleavage was variable between the complexes, with only **Tpd-1a** and **Tpd-1b** inducing cleavage in the visible light range at 365 nm. **Tpd-1b** was additionally capable of cleaving DNA under irradiation at near-IR wavelengths. This effect was not quenched by singlet oxygen scavengers or enhanced in D_2O, indicating that, like some other photoactive naphthalimide compounds (**NN-3a** and **NN-3c**, *vide supra*), the reaction does not proceed *via* a type II pathway as is most common in PDT. Hydroxyl radical scavengers were seen to quench the DNA cleavage activity, which may make **Tpd-1b** useful as a PDT agent.

Complexes **Tpd-2a** and **Tpd-2b** (Fig. 30) contain three naphthalimide moieties on a tetradentate tripodal ligand coordinated to either Fe(III) or Cu(II) centres [134]. Both the free ligand and the complexes were significantly fluorescent with an emission maximum at 480 nm attributed to the excimer of the naphthalimide. Interestingly, this was shown to primarily consist of intramolecular excimers for **Tpd-2a** and **Tpd-2b** as there was almost no change in ratio of the monomer and excimer peaks with change in concentration. In contrast, an increasing concentration of the ligand led to a growth in the excimer peak, suggesting formation of intermolecular excimers instead. Compared to the free ligand, the quantum yields of the complexes were only slightly quenched by the presence of the metal centres. Utilising the fluorescence of **Tpd-2a** and **Tpd-2b** to investigate DNA interaction, both metal complexes were able to moderately displace EtBr while the free ligand did not. DNA binding was theorised to occur primarily at the DNA backbone *via* coulombic interactions, which is in contrast to the typical DNA intercalation observed for naphthalimides [13]. Electrostatic interactions were also thought to contribute to BSA binding, however, binding was primarily driven by hydrophobic interactions. The Cu compound **Tpd-2b** showed higher activity than the Fe(III) equivalent in both DNA- and protein-binding studies possibly because of differences in hydrophobicity (Table S14), charge and geometry. This trend was maintained in cytotoxicity assays using HeLa cells, with **Tpd-2b** being more active with, for example, an IC_{50} value of <5 μM after 48 h of incubation.

3.3.2. *Naphthalimide-bearing porphyrin-derived and other polydentate ligands*

The Zn phthalocyanine derivative **Pht-1a** and its Ga analogue **Pht-1b** (Fig. 31) were reported to be highly luminescent singlet oxygen generators [135] and investigated for their biological properties [136].

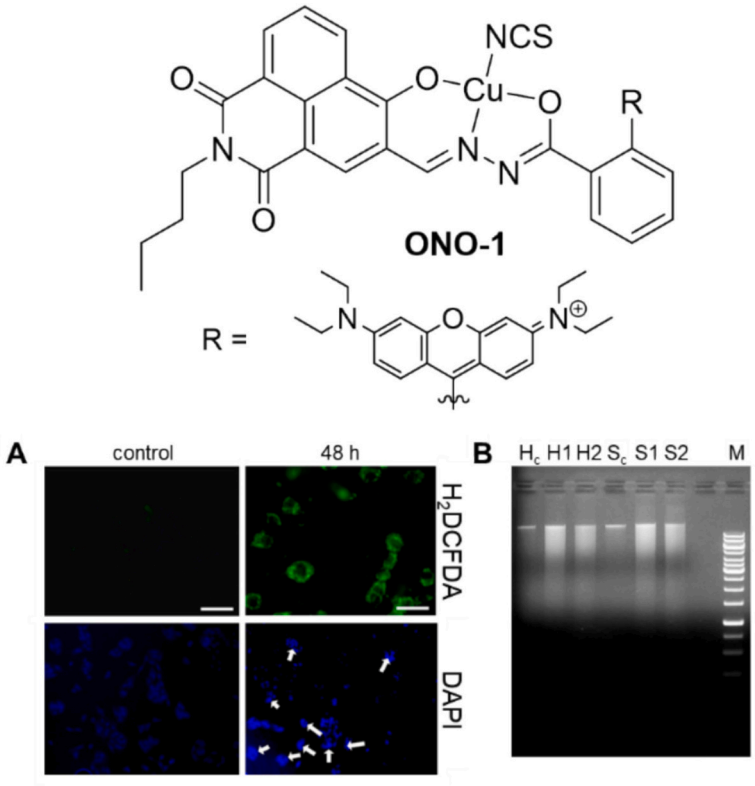

Fig. 29. Chemical structure of the Cu(II) complex **ONO-1** carrying a rhodamine B and naphthalimide conjugate ligand. (**A**) Fluorescence microscopy of HeLa cells treated with **ONO-1** for 48 h at IC_{50} doses and stained with ROS-fluorescent marker dye H_2DCFDA (top) or with DAPI (bottom), for which white arrows show areas of chromatin condensation (scale bar 10 μm). (**B**) DNA gel shift assay showing DNA fragmentation, (M) 1 kb DNA ladder, (H_c) HeLa control, (H1) 24 h and (H2) 48 h treatment of HeLa cells with **ONO-1**; (S_c) SiHa control, (S1) 24 h and (S2) 48 h treatment of SiHa cells with **ONO-1**. Modified from [132] with permission from Elsevier ©2024.

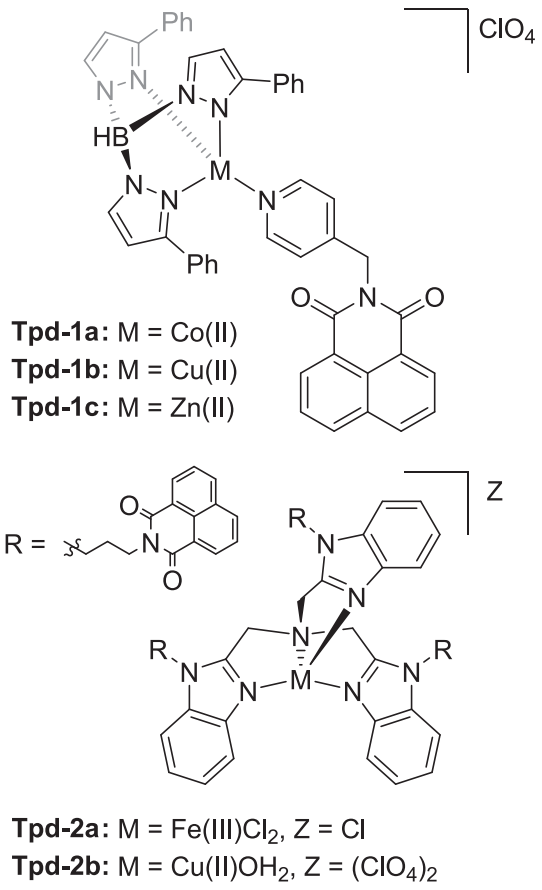

Fig. 30. Complexes with tridentate (**Tpd-1a**–**Tpd-1c**) and tetradentate ligands (**Tpd-2a** and **Tpd-2b**).

Although many phthalocyanines display antioxidant properties, the complexes displayed only modest potency after exposure to the 2,2-diphenyl-1-picrylhydrazyl radical (DPPH). However, in the DNA gel shift assay, both **Pht-1a** and **Pht-1b** were reported to cleave plasmid DNA. The compounds were found to be moderately effective against gram-positive bacteria and showed modest antifungal activity. Irradiating the compounds for 30 min with light before bacterial inoculation improved the activity. This was suggested to be due to ROS production in a PDT-like process.

Zn(II) porphyrin **Por-1** (Fig. 31) carries a naphthalimide moiety on each arm of the porphyrin ligand and self-assembled through nanoprecipitation to form spherical nanoparticles (NPs) of narrow size distribution of *ca.* 60 nm, an ideal size for tumour targeting [137]. *In vitro* cytotoxicity assays were performed for the NPs of **Por-1** and the metal-free porphyrin, finding that both showed photocytotoxicity, which was highest when irradiated by a 635 nm laser and **Por-1** gave an IC_{50} value of 5.86 μg/mL in HeLa cells while showing negligible cytotoxicity in the dark. The cytotoxicity was attributed to a combined effect of ROS production as well as photothermal heating [138].

In another Zn(II) porphyrin, **Por-2** (Fig. 32), the naphthalimide was utilised as a bridging moiety between poly(ethylene glycol) (PEG) and 4,4-difluoro-4-bora-3a,4a-diaza-*s*-indacene (BODIPY) [139]. NPs of the compound were prepared with the aim to enhance its tumour accumulation through the enhanced permeability and retention effect. This effect may result in macromolecular compounds accumulating in solid tumours due to, among other factors, irregular vasculature and impaired lymphatic drainage [140]. **Por-2** gave a broad emission at 580–720 nm in the fluorescence emission spectrum of **Por-2**, which was quenched upon formation of NPs, possibly due to π-stacking interactions. UV–vis spectroscopic titrations with ctDNA revealed that both the complex and

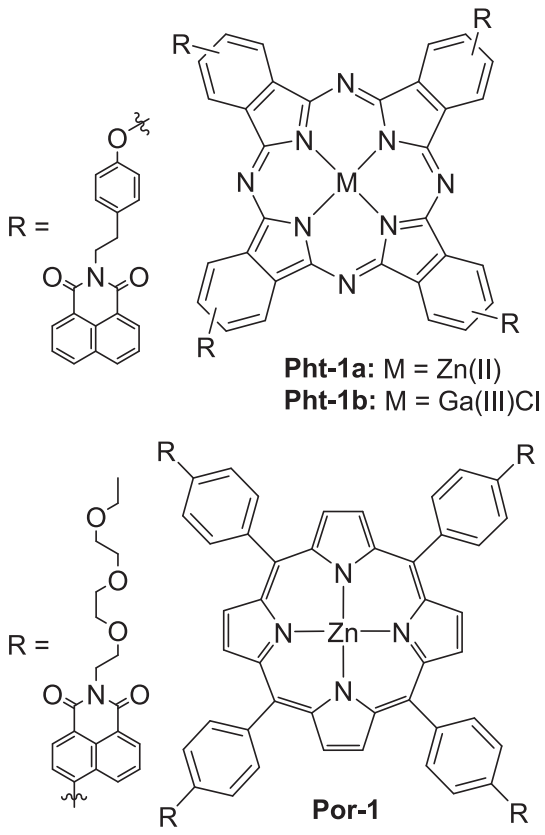

Fig. 31. Structures of the phthalocyanine complexes **Pht-1a** and **Pht-1b** and the porphyrin Zn(II) complex **Por-1**.

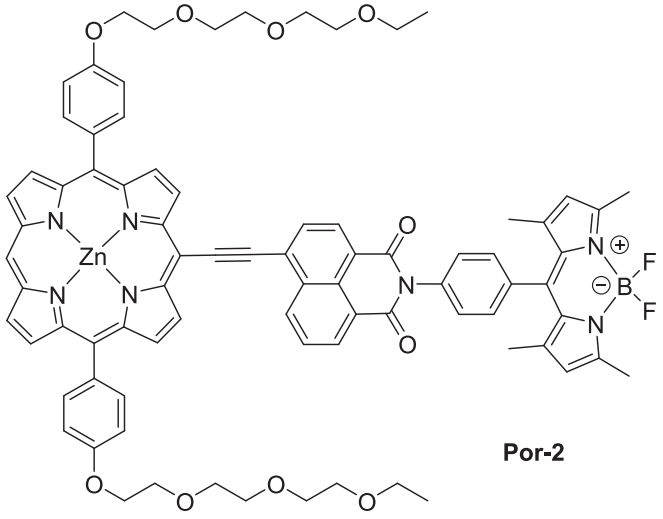

Fig. 32. Structure of naphthalimide porphyrin and BODIPY conjugate **Por-2**.

NPs bound to DNA, with the complex proposed to bind *via* the cationic porphyrin moiety and the NP through non-covalent interactions. Both generated singlet oxygen, although the NPs produced singlet oxygen faster than **Por-2** alone. A significant decrease in cell viability was observed after irradiation of cells treated with the NPs at 680 nm for 10 min.

Of the Cr(III), Co(II), Ni(II), Cu(II) and Zn(II) complexes **Cyc-1a**–**Cyc-1d** bearing cyclam derivatives (Fig. 33) [141], the Cr(III) derivatives generally showed slightly higher antiproliferative activity against cancer cells than the other complexes and was usually in the same range as

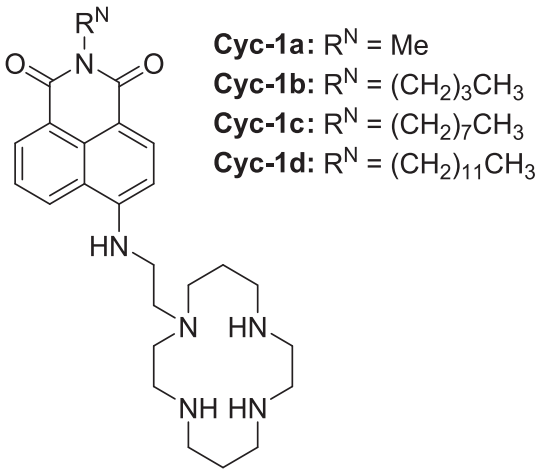

Fig. 33. Structures of ligands **Cyc-1a**–**Cyc-1d**.

the respective ligands. Overall, the reference compound amonafide was more potent, although no standard deviations were provided for the data, and the purity of the compounds was not established beyond high-resolution mass spectrometry (HRMS). The **Cyc-1d** complexes of Zn(II) and Cr(III) were investigated further and the Zn(II) compound was found to inhibit a wide range of receptor tyrosine kinases (RTKs), which are involved in tumour proliferation and angiogenesis, and was found to be antiangiogenic, while being equally toxic across a panel of cancer cell lines assayed.

NPy-1a–**NPy-1c** (Fig. 34) feature a pentadentate ligand to mimic the metal-binding domain of bleomycins, which are natural antibiotics that cause DNA scission and have found clinical use in the treatment of some cancers [142]. In the presence of the external reducing agent dithiothreitol (DTT), **NPy-1b** was least efficient in inducing DNA nicks in supercoiled DNA over 1 h, while **NPy-1a** and **NPy-1c** were similarly effective. In experiments without a reductant present, only **NPy-1a** maintained a moderate extent of DNA-cleaving activity. Despite this, of

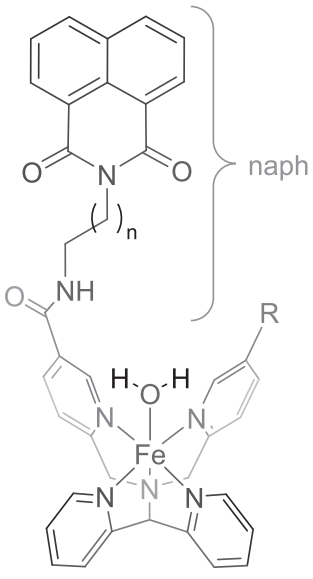

Fig. 34. Structures of complexes **NPy-1a**–**NPy-1c**.

the naphthalimide compounds reported only **NPy-1b** produced strand breaks in double-stranded and single-stranded DNA. From further mechanistic studies, it is likely that the mechanism of damage is through a species formed with either superoxide or hydroperoxide coordinated to the metal centre. Hence, variations in ligand nucleophilicity would have a significant impact on the reactivity of the overall complex, which may be why the ligands which had alkyl amines as the antennae moieties were more active than the naphthalimide derivatives.

3.3.3. *Dendritic structures*

A variety of naphthalimide-metal dendrimers (Figs. 35 and 36) were reported by Grabchev et al., including the poly(propylene imine) (PPI) dendrimers **Dnd-1a**, **Dnd-1b** [143], **Dnd-2a**, **Dnd-2b** [144] and **Dnd-3** [145], and the poly(amidoamine) (PAMAM) dendrimers **Dnd-4** [146], **Dnd-5** [147], **Dnd-6** [148,149], and **Dnd-7** [150].

The PPI dendrimers (Fig. 35) consisted of several generations with naphthalimide termini bearing various R^4 substituents. The dendrimers terminated at the second generation for **Dnd-1a** and **Dnd-1b** [143], the third generation for **Dnd-2a**, and the first generation for **Dnd-2b** [144] and **Dnd-3** [145]. **Dnd-1a** and **Dnd-3** were coordinated to Cu(II), while the other PPI dendrimers were treated with different equivalents of Zn $(NO_3)_2$. While there is no conclusive structural data available, electron paramagnetic resonance (EPR) spectroscopic studies were conducted for **Dnd-1a** and **Dnd-3** to characterise the modes of metal coordination, with results suggesting that they formed bimetallic complexes with Cu $(NO_3)_2$ [143,145]. Antimicrobial testing showed some growth inhibition of *C. candida* along with all the tested bacterial strains, however the minimal inhibitory concentration (MIC) was high for most compounds. The most active compound appeared to be **Dnd-1b** with Zn(II) which resulted in complete inhibition of growth at 38.8 μM for *B. subtilis* and 77.6 μM for *C. lipolytica*. All PPI dendrimers were moderately active in cytotoxicity assays against cancer cells, and **Dnd-3** was found to have some virucidal activity against two different human respiratory viruses.

PAMAM dendrimers (Fig. 36) were reported to form complexes with two equivalents of $Zn(NO_3)_2$ (**Dnd-4**) or $Cu(NO_3)_2$ (**Dnd-5**, **Dnd-6**, **Dnd-7**). The Zn(II) complex of **Dnd-4** [146] was found to have modest inhibitory activity in the gram-negative strains tested and good activity in the gram-positive strains, with the lowest activity seen in gram-negative *E. coli*. This variation in activity could be related to the differences in cell membranes between gram-positive and -negative

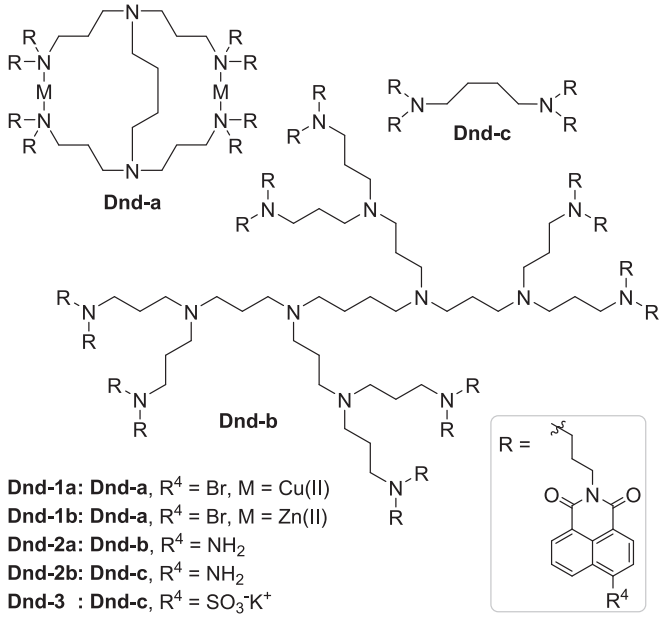

Fig. 35. Cu- or Zn-based metallodendrimers of PPI scaffolds **Dnd-1a**, **Dnd-1b**, **Dnd-2a**, **Dnd-2b**, and **Dnd-3**.

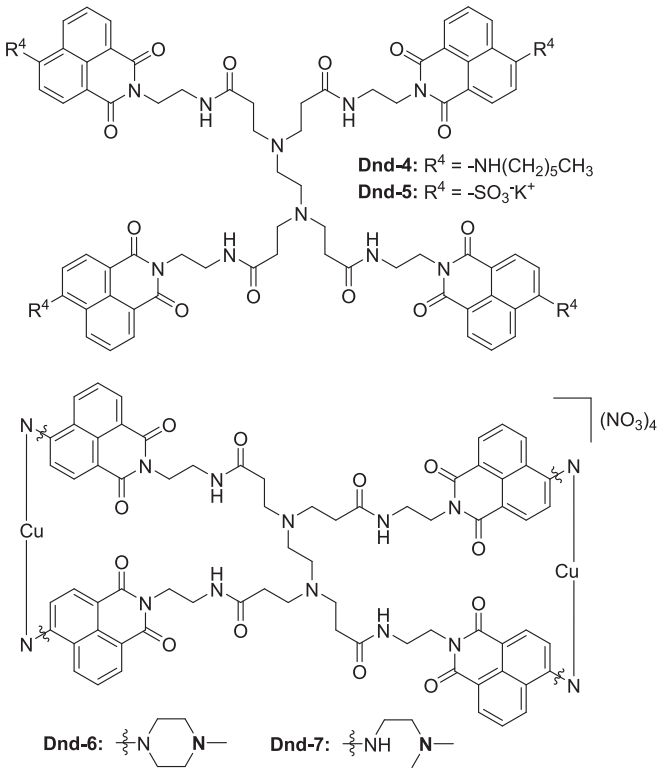

Fig. 36. Dendritic ligands of PAMAM scaffolds forming complexes with Zn$(NO_3)_2$ (**Dnd-4**) or Cu$(NO_3)_2$ (**Dnd-5**, **Dnd-6**, **Dnd-7**). In **Dnd-6** and **Dnd-7** the bolded N-donor atoms coordinate to the Cu centre.

bacteria, with compounds typically requiring greater hydro- or amphiphilic nature to effectively pass through cell membranes of gram-negative bacteria [151]. The Zn(II) complex of **Dnd-4** exhibited slightly higher activity against Hep-2 cancer cells than the metal-free dendrimer, as was also found for Cu$(NO_3)_2$-treated **Dnd-5** [147], which was functionalised with a sulfonate on the naphthalimides rather than alkyl amines found in **Dnd-4**. **Dnd-5** treated with Cu(II) and applied to cotton fabric inhibited *P. aeruginosa* bacterial growth by 39% in the dark and 52% under light irradiation, compared to the free ligand components causing 21–25% growth inhibition in the dark and 33–35% growth inhibition under light irradiation. The antimicrobial activity was suggested to originate from the ability of the metal complex to bind to bacterial membranes and, upon photostimulation, generate singlet oxygen, which may also be the reason for the cytotoxic activity. The compounds were also moderately virucidal, although the metal-free components showed slightly higher activity.

As for the PPI dendrimers, no conclusive structural data was obtained for the PAMAM dendrimers. However, EPR spectroscopic data for **Dnd-6** suggested the coordination geometry around the metal centres to be square planar. The dendrimer ligand also appeared to have significantly lower affinity for Cu(II) than in **Dnd-1a**, which was attributed to the difference in the species functionalised onto the R^4 site of the naphthalimide. The antimicrobial activity of **Dnd-6** was moderate, with a 90% growth inhibition of gram-positive *B. cereus* at 200 μg/mL [148]. However, it also showed significant cytotoxicity in U937 leukaemia cells and much lower growth inhibition in the healthy cell model PBMC, particularly in comparison to the free dendrimer and when dendrimer and Cu(II) were added to cells without pre-formation of the metallodendrimer [149]. As they produced more indiscriminate damage, the ligand and ligand with Cu(II) led to cell death *via* necroptotic processes rather than apoptosis. In contrast, **Dnd-6** affected cell viability more specifically through mitochondrial and lysosomal accumulation and damage, and potentially the interference with or exacerbation of ROS pathways in cancer cells. For the structurally similar **Dnd-7**, cytotoxicity data against MDA-MB-231 cells was reported although issues with aqueous solubility were reported [150] which may have affected both cell and antimicrobial activity studies.

3.3.4. *Schiff base ligands and their complexes*

Schiff bases are frequently employed as ligands in metal complexes, including for such designed to have biological activity [152]. Ligand **Sch-1** (Fig. 37) featuring naphthalimide and Schiff base moieties was coordinated to Co(II) and Cu(II) centres with the structures established with DFT calculations [153]. While the coordination compounds were not characterised, **Sch-1** was reported to be cytotoxic in KHOS-NP osteosarcoma cells, with an IC_{50} value of 35 μM. Of the Schiff base complexes **NO-3a**–**NO-3d** (Fig. 37) [154], **NO-3b** and **NO-3c** were active against gram-negative *K. pneumoniae* and gram-positive *S. aureus*, respectively, at either equal or higher activity than the ciprofloxacin control.

3.3.5. *Unusual ligand systems and organometallics with naphthalimides*

Metallacarborane-naphthalimide conjugates **Cbr-1a**–**Cbr-1f** (Fig. 38) were investigated in HepG2 and RPMI 2650 cancer cells. **Cbr-1c** exhibited a modest IC_{50} value of 29 μM after 24 h incubation in HepG2 and induced intracellular ROS formation and G_0/G_1 arrest [155]. It caused the formation of oxidative DNA lesions at guanosine residues at a level that was significantly higher than that for the mitonafide control, as well as induced mtROS which can damage mtDNA. **Cbr-1c** interacted most strongly with DNA out of the synthesised complexes, however, it still bound much weaker than mitonafide which points towards a different mode of action [155]. Some of the compounds were further tested for their anthelmintic activity, where **Cbr-1a** and **Cbr-1e** were the most active compounds. **Cbr-1e** was also reported as having an IC_{50} value of 14 μM in HT29 colon cancer cells but was non-cytotoxic towards CaCo-2 and LS180 colon cancer cell lines [156]. This may warrant investigation into the specific mode of action of **Cbr-1e** in colon cancer

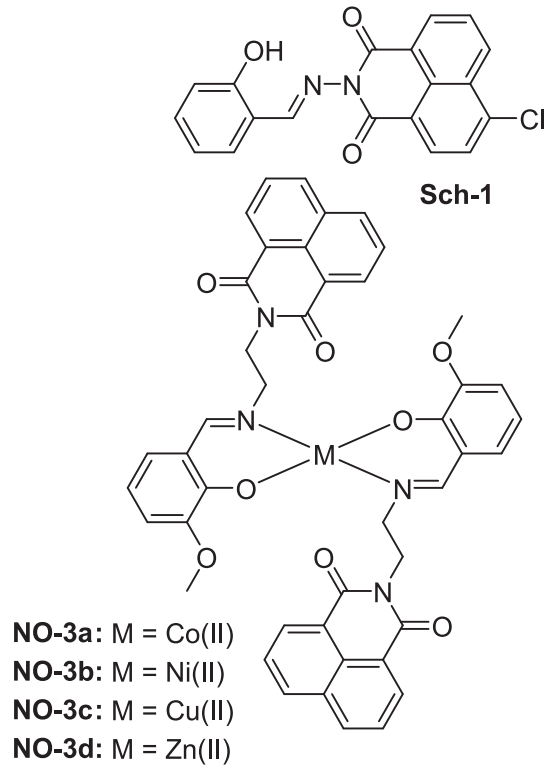

Fig. 37. Structures of Schiff base **Sch-1** and the antibacterial complexes **NO-3a**–**NO-3d**.

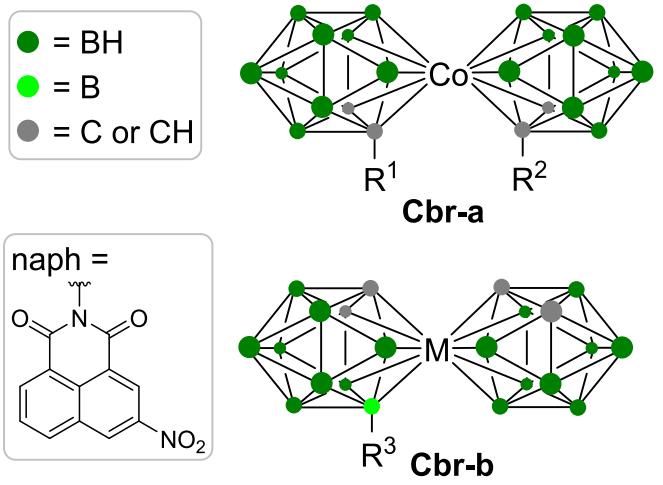

Cbr-1a: Cbr-a, R^1 = Et(naph), R^2 = H
Cbr-1b: Cbr-a, R^1 = Pr(naph), R^2 = H
Cbr-1c: Cbr-a, R^1 = Et(naph), R^2 = $EtNH_2$
Cbr-1d: Cbr-a, R^1 = R^2 = Et(naph)
Cbr-1e: Cbr-b, M = Co(II), R^3 = $[OEt]_2$naph
Cbr-1f : Cbr-b, M = Cr(II), R^3 = $[OEt]_2$naph

Fig. 38. Structures of the metallacarborane complexes **Cbr-1a**–**Cbr-1f**.

cells.

Several ferrocene compounds have demonstrated promising biological activity, with ferroquine being the most prominent example [157,158]. The naphthalimide-appended ferrocene derivatives **Fc-1a**–**Fc-1c** (Fig. 39), **Fc-1c** with a bisnaphthalimide moiety showed stronger DNA binding than the mononaphthalimides **Fc-1a** and **Fc-1b** [159]. Binding of DNA intercalators to DNA typically induces an increase in the viscosity of DNA, however, **Fc-1c** instead caused a decrease in viscosity which suggests it likely interacted through a different mechanism, such as DNA nicking or destabilisation of interstrand interactions [160,161]. **Fc-1c** was reported to be the most cytotoxic compound while **Fc-1a** was non-cytotoxic in all cancer cell lines tested.

Utilising the same overall structure as for **Fc-1c**, a range of bisnaphthalimide compounds **Fc-2a**–**Fc-2h** (Fig. 39) was prepared by varying the lengths of the alkyl spacers between the naphthalimide and ferrocene moieties [162]. **Fc-2a** bearing the shortest linker, and thus the most similar structurally to **Fc-1c**, was found to exhibit the strongest binding affinity towards ctDNA. No distinct relationship was observed between compound linker length and DNA binding affinity, which may be due to the overall small degree of variation in activity between the compounds. Considering the relatively high similarity of the compounds both in their structure as well as their affinity for binding DNA, it is not surprising that the cytotoxicity of the compounds was also very similar and in the low micromolar range for the four cancer cell lines tested. There was one notable exception, however, with **Fc-2a** having an IC_{50} value of 0.4 μM in the HepG2 hepatocellular carcinoma cell line, a ten-fold increase compared to its activity in the three other cell lines, and a five-fold increase compared to **Fc-2g** with second highest activity in HepG2. **Fc-2b** and **Fc-2e** were found to localise more in cytosol of HepG2 cells and exhibited IC_{50} values of ~3 μM, while **Fc-2a** in comparison had higher uptake in nuclei and was also found to increase levels of cellular ROS in a dose-dependent manner. Further studies could seek to investigate the mechanisms by which **Fc-2a** exerts its antiproliferative effect on hepatocellular carcinoma, such as probing the relationship between DNA binding affinity and cytotoxicity.

Of the ferrocene-functionalised naphthalimide derivatives **Fc-3a**–**Fc-3h** (Fig. 40), **Fc-3f** was found to exert strong growth inhibition towards MCF-7 cells within 48 h with a GI_{50} value of 8.0 μM [163]. However, at 72 h it was inferior compared to the structure lacking the ferrocene moiety which gave a GI_{50} value of ~2.2 μM. Several of the compounds did not reach the GI_{50} value in MCF-7 cells within 24 or even 48 h, hence these compounds were identified as ideal candidates for cellular imaging applications. Other ferrocene compounds substituted with naphthalimide were reported as intracellular turn-on fluorescent probes for GSH, showing only mild cytotoxicity within the time required for staining [164,165].

The only reported naphthalimide-functionalised anticancer agent with a Mn centre **NNN-4** (Fig. 42) is a photocytotoxic lysosome-targeted Mn(I) compound [166] that is able to act as a CO-releasing molecule (CORM) [167]. It was designed to be photoactive, releasing the CO ligands upon irradiation in aqueous solution to form the triaqua species and then inducing singlet oxygen formation as well as naphthalimide-centred fluorescence [166]. A gradual increase in fluorescence at 546 nm was observed following intermittent radiation at 405 nm over 35 min, attributed to the release of the CO ligands which was then confirmed *via* IR spectroscopic measurements (Fig. 42). This process was not affected by dithionite as a reductant and could be triggered by H_2O_2,

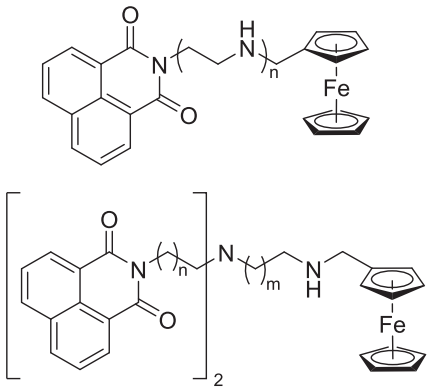

Fc-1a: n = 1
Fc-1b: n = 2

Fc-1c: n = m = 1
Fc-2a: n = 1, m = 2
Fc-2b: n = 1, m = 3
Fc-2c: n = 2, m = 1
Fc-2d: n = 2, m = 2
Fc-2e: n = 2, m = 3
Fc-2f : n = 2, m = 4
Fc-2g: n = 3, m = 2
Fc-2h: n = 4, m = 2

Fig. 39. Ferrocene-functionalised naphthalimides **Fc-1a**–**Fc-1c** and **Fc-2a**–**Fc-2h**.

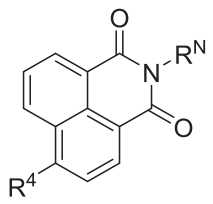

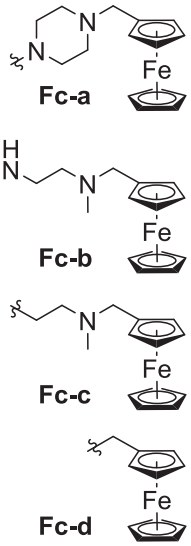

Fc-3a: R^N = Me, R^4 = **Fc-a**
Fc-3b: R^N = Me, R^4 = **Fc-b**
Fc-3c: R^N = **Fc-c**, R^4 = **Fc-b**
Fc-3d: R^N = **Fc-d**, R^4 = NHEtNHMe
Fc-3e: R^N = **Fc-d**, R^4 = ppz
Fc-3f : R^N = **Fc-d**, R^4 = ppz(N-Me)
Fc-3g: R^N = **Fc-d**, R^4 = $NHEtNMe_2$
Fc-3h: R^N = **Fc-d**, R^4 = NHEt(N-mor)

Fig. 40. Ferrocene-functionalised naphthalimides **Fc-3a**–**Fc-3h** (ppz = piperazine).

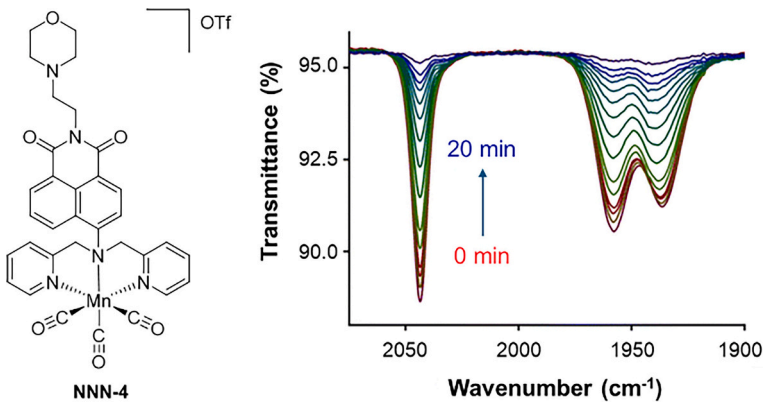

Fig. 42. Structure of the Mn(I) complex **NNN-4** and changes in the IR spectra of **NNN-4** (10 mM) during irradiation every 2 min in phosphate-buffered saline (PBS). Reprinted from [166] with permission from the Royal Society of Chemistry ©2024 https://doi.org/10.1039/D4CC00009A.

although at a much lower rate than observed with irradiation, which can be favourable in the highly reducing tumour environment. Cytotoxicity assays in HeLa cells and the healthy cell model NIH-3T3 indicated low potency of **NNN-4** in the dark in both cell types. While irradiation activated the compound in the cancer cells, **NNN-4** retained low activity in NIH-3T3 upon irradiation.

Cu(II) and Zn(II) complexes of the morpholine-functionalised ligand **Mor-1** (Fig. 43) were investigated for antibacterial activity against gram-negative *A. calcoaceticus* and antifungal activity against *S. cerevisiae* and *C. lipolytica* [168]. The Cu complex showed slightly higher activity than the Zn derivative in all these microorganisms.

3.4. Naphthalimides in other metal complexes

The platinum group elements are a rich source when it comes to developing compounds with biological activity. This ranges from the archetypical Pt complexes discussed to Au and Ir coordination compounds and organometallics with anticancer, antibacterial, and other biological properties [157,169,170]. The prototype Au compound auranofin has shown applicability in a diverse range of biological applications [171] and remains in various phases of clinical trials for treatment of cancer and other conditions [172,173].

3.4.1. Gold compounds

Au(NHC) complexes have been explored as anticancer agents [174] and **NHC-5a**–**NHC-5f** (Fig. 44) were developed by Ott et al. as analogues of various NHC metal complexes of Ru, Rh, Ag, and Cu (*vide supra*). The bisnaphthalimide Au(I) complexes **NHC-5e** and **NHC-5f** were significantly less cytotoxic than the pro-carbenes [103]. However, the mononaphthalimide complexes **NHC-5a**–**NHC-5d** (Fig. 44) were more active, with the thioalkyl derivative **NHC-5d** showing particularly high

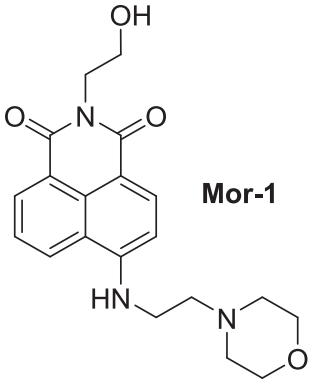

Fig. 43. Structure of ligand **Mor-1**, used to prepare Cu and Zn complexes.

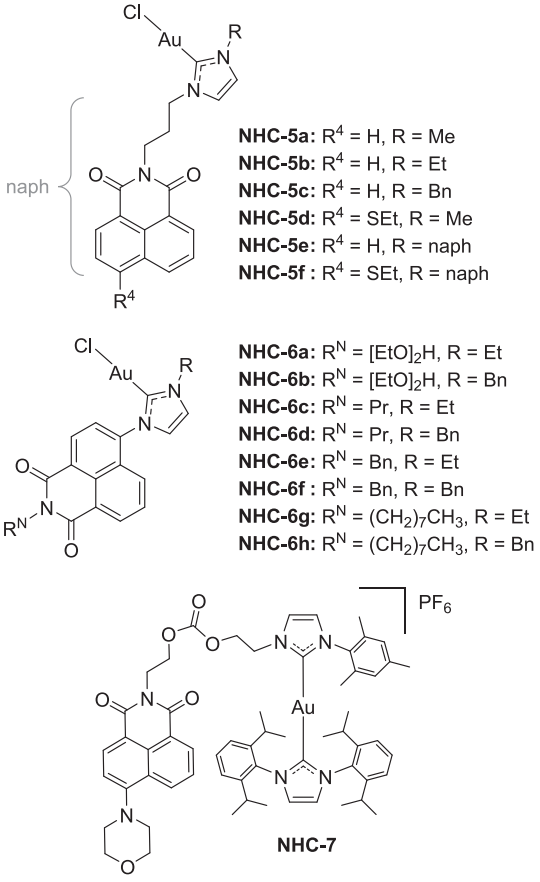

Fig. 44. Structures of Au(I) NHC complexes with R^N- (**NHC-5a**–**NHC-5f**) and R^4-substituted naphthalimides (**NHC-6a**–**NHC-6h**) as well as of the bis-NHC Au complex **NHC-7**.

inhibitory activity against HT-29 and MCF-7 cancer cells as well as of thioredoxin reductase, the natural target of Au complexes due to the selenocysteine moiety [175]. It was further found to decrease cellular respiration, cell impedance and extracellular acidification in a dose-dependent manner which was not reversible after removing the drug-containing medium. The cytotoxicity increased across **NHC-5a**–**NHC-5c** as the second NHC substituent increased in steric bulk, while no such trend was seen for the pro-carbenes. While **NHC-5a** was not the most potent cytotoxin nor thioredoxin reductase inhibitor, it intercalated into DNA more effectively than any of the other complexes. Interestingly, the relationship between steric bulk at the NHC and efficacy of DNA

intercalation in the complexes was found to be increase with steric bulk to the degree that the pro-carbene of **NHC-5c** showed a similar efficacy to **NHC-5a** [106]. This could indicate that the other substituent on the endocyclic NHC nitrogen atom has an influence on the DNA-binding efficacy of the naphthalimide fragment.

Complexes **NHC-6a**–**NHC-6h** (Fig. 44) were developed as cytotoxic cellular bioimaging agents with varying substituents on both the naphthalimide and NHC nitrogen atoms [107]. Most of the metal complexes were largely non-cytotoxic in the cancer cell lines tested but **NHC-6h** showed an IC_{50} value of 4.8 μM in MCF-7 cells despite being non-cytotoxic in A549 and PC3. The bis-NHC complex **NHC-7** (Fig. 44) incorporates a naphthalimide moiety in an asymmetrically substituted NHC ligand [108]. Preliminary *in vitro* studies were performed to investigate the cytotoxicity and intracellular localisation of **NHC-7** in A549 lung cancer cells. It was found to localise in mitochondria both with and without BSA present and gave an IC_{50} value in the nM range which was more potent than auranofin.

Complexes **S-1a**–**S-1d** feature a similar coordination motif to auranofin with thioglucose replaced with a thiolate-functionalised naphthalimide (Fig. 45), which resembles to some extent amonafide and mitonafide with their R^N substituent [109,176]. The cytotoxicity of **S-1a**–**S-1d** in HT-29 and MCF-7 increased with higher lipophilicity of the PR_3 ligand coordinated to the Au centre. This was also true for the analogous $(R_3P)AuCl$ complexes, but the naphthalimide-functionalised complexes were in general more cytotoxic than the respective chlorido equivalents. The complex type is able inhibit thioredoxin reductase, as was demonstrated for **S-1b**, possibly through binding to selenocysteine or cysteine residues, as would be expected for Au(I) anticancer agents of this type. Furthermore, it was found that **S-1b** strongly induced apoptosis at concentrations as low as 2.5 μM, and decreased the mitochondrial membrane potential at even lower concentrations, indicating that apoptosis may be induced through a mitochondrial pathway [176]. **S-1b** and **S-1d** inhibited angiogenesis in zebrafish embryos while the chlorido equivalents did not, providing evidence for the activity arising from the naphthalimide moiety. In an antiangiogenesis assay in zebrafish embryos (Fig. 45), **S-1d** inhibited tumour-cell induced neovascularisation [109].

3.4.2. *Organoiridium compounds*

The bipyridine complexes **NN-10a**–**NN-10c** (Fig. 46) were reported alongside Ru(II) complex **NN-8** (*vide supra*). **NN-10b** and **NN-10c** showed moderate to high activity in *in vitro* anticancer activity assays while **NN-10a** and **NN-8** were inactive [113]. However, they were similarly active in the healthy cell model BEAS-2B with the exception of **NN-10c**. This discrimination of activity could be related to several factors including the stronger ability of **NN-10b** to bind to BSA compared to **NN-10c**. Furthermore, significant difference in their cellular distribution was found with **NN-10b** largely accumulating in mitochondria and its cell uptake appeared to be energy-dependent, while **NN-10c** primarily localised in lysosomes. In A549 cells, **NN-10c** seemed to lead to

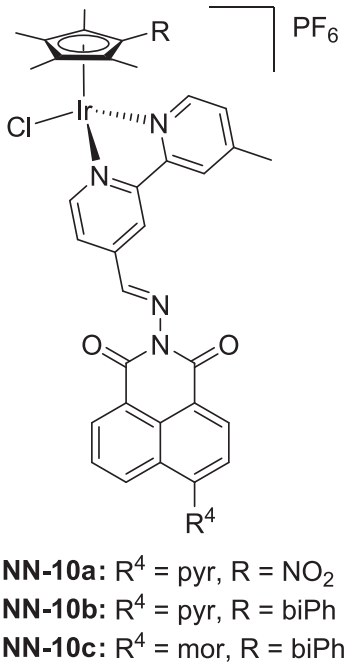

Fig. 46. Chemical structures of the Ir(I) complexes **NN-10a**–**NN-10c** (pyr = pyrrolidine, mor = morpholine, biPh = biphenyl).

lysosomal rupture and cell death may be induced through lysozyme permeabilisation of cell membranes. Conjugation of a morpholine fragment to the naphthalimide moiety has previously also shown to result in lysosome targeting for the Ru(II) complex **N-9a** (*vide supra*) [114], while introduction of morpholine is frequently applied in medicinal chemistry to alter the solubility properties of compounds [177].

NN-10b was further investigated in A549 cells for ROS production, cell cycle arrest, pro-apoptotic, and antimetastatic activity [113]. In a dose-dependent manner, it induced cell cycle arrest in S and G_2/M phases and caused cell death through apoptosis rather than necrosis. It also exhibited significant antimetastatic activity at the IC_{50} concentration, reducing wound healing by almost 95% at 24 h. **NN-10b** was further found to induce intracellular ROS. The damage to mitochondria was widespread and resulted in the majority being phagocytosed by lysosomes after 24 h of treatment.

The Ir(III) compound **NN-11** (Fig. 47) was designed as a PS agent for PDT. It was conjugated to upconverting NPs ($NaYF_4$:Yb/Tm@$NaYF_4$) [178] while the HIF-1α inhibitor YC-1 was adsorbed on the NPs. The lanthanide-doped NPs were utilised with the aim to enable PDT of **NN-11** as Ir(III) complexes typically absorb poorly in the near-infrared region. Lanthanide NPs can thus convert near-infrared radiation to a higher-energy visible wavelength to activate the Ir(III) complex. The

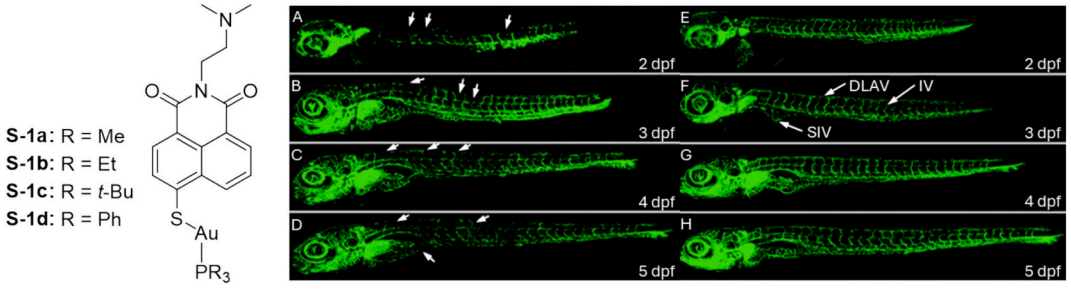

Fig. 45. Structures of auranofin derivatives **S-1a**–**S-1d**. Inhibition of angiogenesis in zebrafish embryos from 2 to 5 d post-fertilisation (dpf). The embryos were treated with 0.05 μM of either **S-1d** (panels A–D) or the chlorido equivalent (panels E–H); intersegmental vessel (IV), dorsal longitudinal anastomic vessel (DLAV) and subintestinal vein (SIV). Arrows indicate vessel defects in embryos treated with **S-1d**. Modified from reference [109] with permission from the Royal Chemical Society ©2009.

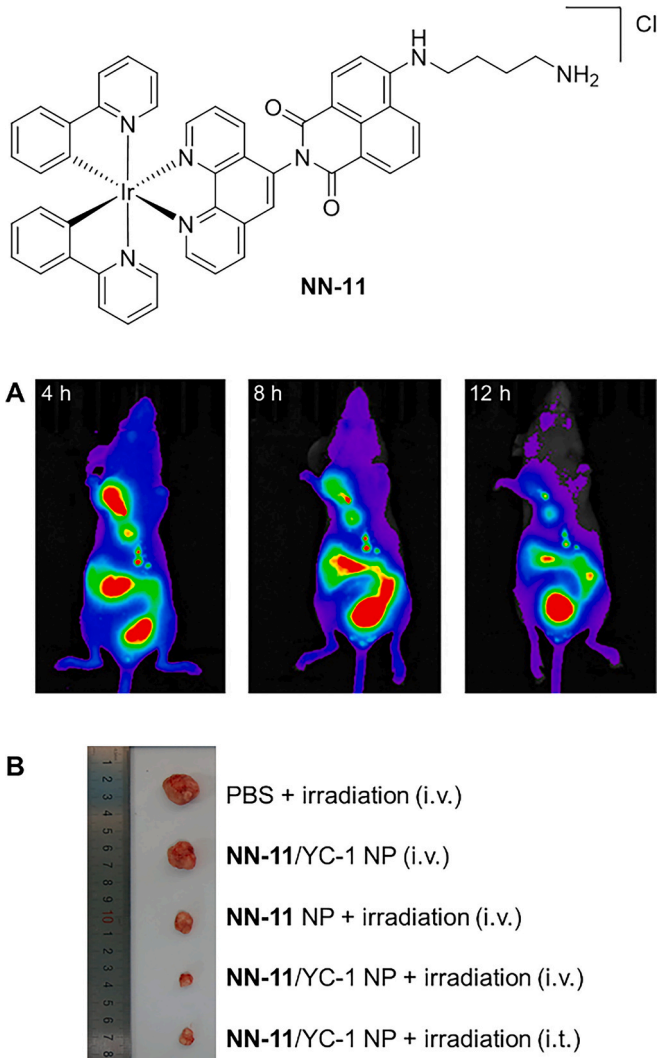

Fig. 47. Structure of **NN-11**. (**A**) *In vivo* fluorescence tumour imaging in mice 4, 8, and 12 h after intravenous injection of **NN-11**/YC-1 NPs. (**B**) Representative photographs of excised tumours at 27 d post-treatment under different conditions. Modified from [178] with permission by the American Chemical Society ©2020.

naphthalimide moiety acted as an antenna to optimise energy uptake of the metal complex. The emission peak of **NN-11** was red-shifted by ~30 nm compared to the analogous Ir complex without the naphthalimide moiety, with a phosphorescence lifetime approximately 1 μs longer. Unfortunately, the phosphorescence quantum yield also decreased from 41% to 6.5%. However, **NN-11** was significantly more effective than $[Ru(bipy)_3]Cl_2$, at producing singlet oxygen in normoxia and also caused singlet oxygen formation under hypoxic conditions, although at a lower efficiency. DFT calculations suggested that the lowest triplet excited state of **NN-11** involves an intraligand triplet excited state transition from the naphthalimide to the phenanthroline. This supports that the naphthalimide could be used as a light harvester to activate the PS activity at the metal centre. Upon conjugation to the upconverting NPs and after irradiation at 980 nm, the NP-centred fluorescence emission bands, which overlapped with the naphthalimide absorption bands in the visible region, were significantly quenched, indicating energy transfer to the naphthalimide moiety. *In vitro* cytotoxicity assays showed that in normoxia both the NPs with and without YC-1 were considerably cytotoxic and a similar percentage of cells undergoing apoptosis or necrosis (~46%). In hypoxic conditions however, the NPs loaded with YC-1 became more potent. Results were similar for *in vivo* studies in murine models, where tumour size significantly decreased after treatment with **NN-11**/YC-1 nanoparticles over 27 d (Fig. 47), when the drug was administered every 7 d. Intratumoural (i.t.) administration of the agent produced only marginally improved results compared to that for intravenous (i.v.) injection, which has significantly more applicability for clinical use.

3.4.3. *Sn complexes*

Organotin(IV) compounds have been investigated as antitumour and bioimaging agents, with moieties coordinating to Sn(IV) typically retaining their fluorescence, which is unlike what is often seen for transition metal complexes [179]. To the best of our knowledge, there is only one report of organotin(IV) naphthalimide compounds as anticancer agents. Complexes **O-8a**–**O-8c** (Fig. 48) showed higher fluorescence intensity in the solid state compared to the free naphthalimide ligand, with **O-8c** showing the most intense emission which was also markedly blue shifted [180]. Preliminary cytotoxicity assays were performed in MCF-7 and HepG2 cancer cells, in which the free naphthalimide ligand was only moderately cytotoxic at 45 and 19 μM, respectively, while the complexes gave IC_{50} values in the high nanomolar range.

4. Conclusions

Metal complexes are a mainstay in cancer chemotherapy and equipping them with uncommon or multiple modes of action is aimed to overcome shortcomings of current chemotherapeutics. Due to numerous organic naphthalimide compounds with promising biological properties, diverse metal complexes incorporating naphthalimide moieties have been reported in attempts to alter the properties of bioactive metal complexes, including those of clinically used cisplatin and oxaliplatin. In addition, developmental anticancer agents based on Pt, Pd, Ru, Au, Ag, Rh, Ir, Fe, Ga, Zn, Cu, Co, Ni, Cr and Sn were reported (Fig. 49) although not all of them are fully characterised both in terms of structure and purity. Nevertheless, several examples exhibited promising properties with sometimes unconventional modes of action. The effect of naphthalimide conjugation to metal fragments is not always clear in terms of impact on the biological activity. Surprisingly, conjugation of more than

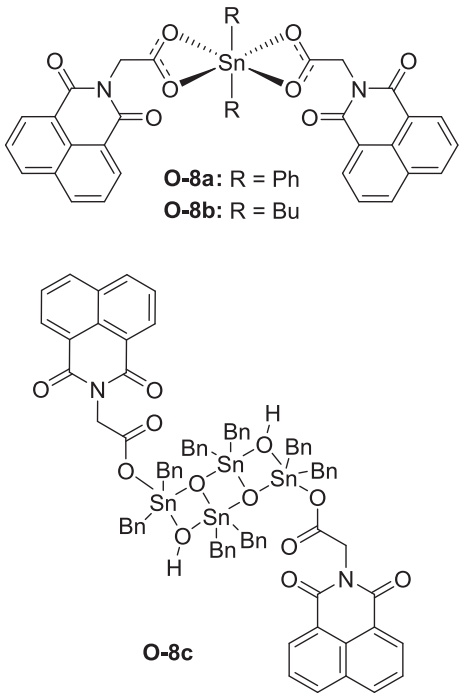

Fig. 48. Structures of Sn(IV) complexes **O-8a**–**O-8c**.

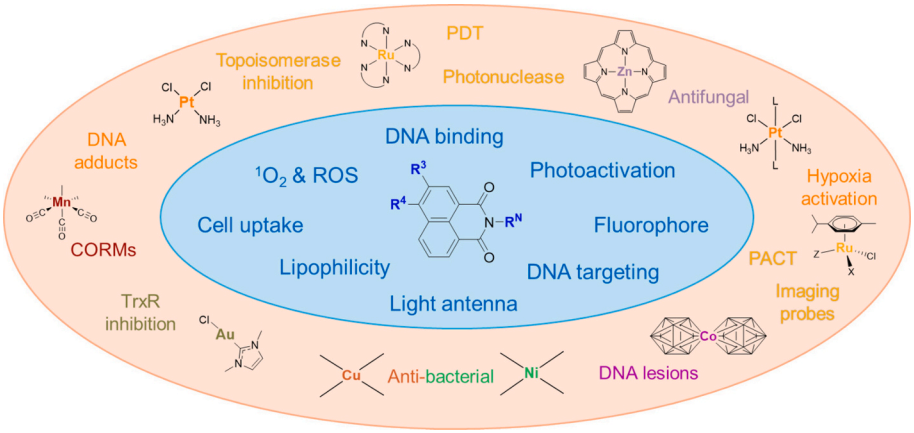

Fig. 49. Modes of action, design concepts and structural diversity of naphthalimide-functionalised metal complexes with biological activity.

one naphthalimide fragment per metal moiety generally gave reduced activity, with the exception being some complexes with polydentate ligands. Although the overall relationship is not always obvious and the number of cell studies under comparable conditions is limited, in general incorporating a naphthalimide moiety in a metal complex was found to be a successful strategy to improve the biological activity, in particular the cytotoxicity in cancer cells, as for example found for cisplatin-derived naphthalimide-bearing Pt(II) and Pt(IV) complexes. As for many other compound classes, the comparison of biological activity in cancer cells and 'healthy', non-tumourigenic cells is common practice, but the relevance of such cell models for predicting the existence of a therapeutic window is contested. This is supported by the fact that most compounds discussed here are more active in cancer cells than the 'healthy' variants.

The functionalisation of complexes with naphthalimide was found to significantly alter the physicochemical properties of metal complexes. The considerable lipophilic nature of the naphthalimide moiety likely exerts significant influence on localisation as well as the large variability in biological effect of these compounds, with a delicate balance between lipophilicity and aqueous solubility. The precise degree of lipophilicity either tolerated or even required for activity varies significantly between metal complexes of different overall structure, with few studies delving further into structure-activity relationships, which is another limitation to establish clear-cut generalisable structure-activity relationships for the compound class. In addition, progress has been made in understanding that ligand design and metal choice are essential to achieve the desired biological properties. This is particularly essential for naphthalimide conjugation which requires introduction of mono-, bi- or multidentate donor systems to form sufficiently stable complexes with metal centres, allowing their use in biologically relevant media. The denticity of the ligand will also control the stability of the complex, which is further affected by the choice of co-ligands that may be selected to allow for additional interactions of the metal centre with biological molecules through dative covalent bond formation.

An advantage of naphthalimide functionalisation is the photochemical properties they bring with them. This may hold potential for fluorescence imaging, photodynamic therapy and photoactivated chemotherapy. However, these applications are very much dependent on the effect of metal coordination on the photophysical properties, which frequently have not been fully characterised in detail, including the type of luminescence exhibited by the complexes. A few examples have been reported so far where these concepts have been successfully implemented, most notably for PACT or PDT, utilising established concepts of activating metal–ligand bonds. Induction of ROS formation was often driven by metal fragments, with the naphthalimide moiety observed to increase ROS yields and the overall activity of the complexes.

The DNA binding ability was frequently investigated for the compounds and many examples were found to bind to nucleic acids or other biological macromolecules in the test tube. However, the compounds did not necessarily accumulate in cell compartments with high nucleic acid content, nor did high DNA affinity correlate with cytotoxicity in cancer cell models. While DNA interaction experiments usually indicated intercalation, which is typical for naphthalimides, metal moieties equip them with novel, uncommon biological properties. However, this also results in the modes of action for naphthalimide-functionalised metal complexes often being poorly understood and characterised beyond any structural relationships.

A limitation in the biological studies on naphthalimide-functionalised metal complexes is that a wide range of models and methods were utilised to investigate the various biological activities of the compounds, which makes it difficult to compare data collected from different research groups. Nevertheless, the breadth of biological activities described for the various naphthalimide complexes, shows the promise these structures hold. In addition to anticancer activity, there are several reports on potential use as antibacterial, antifungal, virucidal, and nematicidal agents. Unfortunately, only a very limited number of studies investigated the activity of the compounds *in vivo*, however, studies which did utilise *in vivo* experiments found the prepared naphthalimide-metal complexes to be safe and effective in mice against tumours of various origins. On the other hand, in some cases the free naphthalimide ligands yielded equal or greater cytotoxicity than the metal complexes, which could have several reasons, including altered cellular uptake, intracellular distribution and an effect of *in vitro* speciation of formed complexes. Addition of the naphthalimide moiety may yield complexes which accumulate in different tissues or cell compartments, with various substitutions on the naphthalimide capable of influencing localisation. Ligand exchange kinetics may contribute to this effect, and studies to establish speciation in the aqueous environment may aid to probe suitability for those frameworks where aquation or other ligand exchange is anticipated to be required for biological activity.

Overall, despite encouraging biological results and the interesting physicochemical properties endowed by naphthalimides on metal complexes, there is still significant work to be done to develop the compound class to their full potential. The most promising approach to fully realise the potential of naphthalimide appears to be based on their incorporation into scaffolds of metal compounds with well-established biological properties.

Declaration of competing interest

The authors declare that they have no known competing financial interests or personal relationships that could have appeared to influence

the work reported in this paper.

Acknowledgements

This project was supported by the Aotearoa New Zealand Tāwhia te Mana Research Fellowships, administered by the Royal Society Te Apārangi, and the MacDiarmid Institute for Advanced Materials and Nanotechnology. J. S. thanks the University of Auckland for a doctoral scholarship, and C. G. H. the Alexander von Humboldt Foundation for a Humboldt Research Award.

Appendix A. Supplementary data

Supplementary data to this article can be found online at https://doi.org/10.1016/j.ccr.2026.217899.

Data availability

No data was used for the research described in the article.

References

[1] S. Banerjee, E.B. Veale, C.M. Phelan, S.A. Murphy, G.M. Tocci, L.J. Gillespie, D. O. Frimannsson, J.M. Kelly, T. Gunnlaugsson, Chem. Soc. Rev. 42 (2013) 1601–1618.
[2] A. Kamal, N.R. Bolla, P.S. Srikanth, A.K. Srivastava, Expert Opin. Ther. Pat. 23 (2013) 299–317.
[3] H.-Q. Dong, T.-B. Wei, X.-Q. Ma, Q.-Y. Yang, Y.-F. Zhang, Y.-J. Sun, B.-B. Shi, H. Yao, Y.-M. Zhang, Q. Lin, J. Mater. Chem. C 8 (2020) 13501–13529.
[4] U. Duraisamy, Recent Innov, Chem. Eng. 13 (2020) 262–289.
[5] H. He, M.A. Mortellaro, M.J.P. Leiner, R.J. Fraatz, J.K. Tusa, J. Amer. Chem. Soc. 125 (2003) 1468–1469.
[6] M.D. Tomczyk, K.Z. Walczak, Eur. J. Med. Chem. 159 (2018) 393–422.
[7] R. Tandon, V. Luxami, H. Kaur, N. Tandon, K. Paul, Chem. Rec. 17 (2017) 956–993.
[8] J. Gao, J. Chapman, Drug Dev. Res. 84 (2020) 1–10.
[9] E.R.T. Tiekink, I.M. Scharfbillig, B.F. Hoskins, J.M. Gulbis, C.J. Easton, Z. Kristallogr, Cryst. Mater. 199 (1992) 249–254.
[10] J.A. Kitchen, R. Parkesh, E.B. Veale, T. Gunnlaugsson, Luminescent Sensing, in: P. A. Gale, J.W. Steed (Eds.), Supramol. Chem, John Wiley & Sons, Ltd., Chichester, UK, 2012.
[11] J.I. Lovitt, C.S. Hawes, A.D. Lynes, B. Haffner, M.E. Möbius, T. Gunnlaugsson, Inorg. Chem. Front. 4 (2017) 296–308.
[12] R. Goel, S. Sheryl, P. Kamaldeep, L. Vijay, Sens. Actuators B 246 (2017) 776–782.
[13] M.F. Braña, M. Cacho, A. Gradillas, B.d. Pascual-Teresa, A. Ramos, Curr., Pharm, Des 7 (2001) 1745–1780.
[14] Y. Liu, J.T. Norton, M.A. Witschi, Q. Xu, G. Lou, C. Wang, D.H. Appella, Z. Chen, S. Huang, Neoplasia 13 (2011) 453–460.
[15] J.T. Norton, M.A. Witschi, L. Luong, A. Kawamura, S. Ghosh, M. Sharon Stack, E. Sim, M.J. Avram, D.H. Appella, S. Huang, Anticancer Drugs 19 (2008) 23–36.
[16] R. Levitt, J.C. Buckner, T.L. Cascino, P.A. Burch, R.F. Morton, M.W. Westberg, R. M. Goldberg, J.G. Gallagher, J.R. O'Fallon, B.W. Scheithauer, J. Neurooncol 23 (1995) 87–93.
[17] M.J. Ratain, G. Rosner, S.L. Allen, M. Costanza, D.A.V. Echo, I.C. Henderson, R. L. Schilsky, J. Clin. Oncol. 13 (1995) 741–747.
[18] G. Gellerman, Lett. Drug Des. Discov. 13 (2016) 47–63.
[19] M.B. Murphy, S.L. Mercer, J.E. Deweese, Chapter five - inhibitors and poisons of mammalian type II topoisomerases, in: J.C. Fishbein, J.M. Heilman (Eds.), Advances in Molecular Toxicology, Elsevier, Netherlands, 2017, pp. 203–240.
[20] P. De Isabella, F. Zunino, G. Capranico, Nucleic Acids Res. 23 (1995) 223–229.
[21] M.F. Braña, J.M. Castellano, M. Morán, M.J. Pérez de Vega, C.R. Romerdahl, X. D. Qian, P. Bousquet, F. Emling, E. Schlick, G. Keilhauer, Anticancer Drug Des. 8 (1993) 257–268.
[22] M.F. Braña, J.M. Castellano, M. Morán, M.J. Pérez de Vega, D. Perron, D. Conlon, P.F. Bousquet, C.A. Romerdahl, S.P. Robinson, Anticancer Drug Des. 11 (1996) 297–309.
[23] M.F. Braña, A. Ramos, Curr. Med. Chem. Anticancer Agents 1 (2001) 237–255.
[24] P.F. Bousquet, M.F. Braña, D. Conlon, K.M. Fitzgerald, D. Perron, C. Cocchiaro, R. Miller, M. Moran, J. George, X.-D. Qian, G. Keilhauer, C.A. Romerdahl, Cancer Res. 55 (1995) 1176–1180.
[25] A. Awada, R. Thödtmann, M.J. Piccart, J. Wanders, A.H. Schrijvers, I.M. Von Broen, A.R. Hanauske, Eur. J. Cancer 39 (2003) 742–747.
[26] S. O'Reilly, S.D. Baker, S. Sartorius, E.K. Rowinsky, M. Finizio, G.M. Lubiniecki, L. B. Grochow, J.E. Gray, H.I. Pieniaszek, R.C. Donehower, Ann. Oncol. 9 (1998) 101–104.
[27] J. Thompson, C.B. Pratt, C.F. Stewart, L. Avery, L. Bowman, W.C. Zamboni, A. Pappo, Invest. New Drugs 16 (1998) 45–49.
[28] R.J. Cherney, S.G. Swartz, A.D. Patten, E. Akamike, J.-H. Sun, R.F. Kaltenbach, S. P. Seitz, C.H. Behrens, Z. Getahun, G.L. Trainor, M. Vavala, M.R. Kirshenbaum, L. M. Papp, M.P. Stafford, P.M. Czerniak, R.J. Diamond, R.J. McRipley, R.J. Page, J. L. Gross, Bioorg. Med. Chem. Lett. 7 (1997) 163–168.
[29] P.K. Chatterjee, N.L. Sternberg, Proc. Natl. Acad. Sci. U. S. A. 92 (1995) 8950–8954.
[30] J.L. Nitiss, J. Zhou, A. Rose, Y. Hsiung, K.C. Gale, N. Osheroff, Biochemistry 37 (1998) 3078–3085.
[31] S.F. Chen, D.L. Behrens, C.H. Behrens, P.M. Czerniak, D.L. Dexter, B.L. Dusak, J. R. Fredericks, K.C. Gale, J.L. Gross, J.B. Jiang, K.M.R.J. McRipley, L.M. Papp, A. D. Patten, F.W. Perrella, S.P. Seitz, M.P. Stafford, J.H. Sun, T. Sun, M.A vol. 4, Hoff, Anti-Cancer Drugs, Wuonola, D.V, 1993, pp. 447–458.
[32] M.R. Kirshenbaum, S.-F. Chen, C.H. Behrens, L.M. Papp, M.M. Stafford, J.-H. Sun, D.L. Behrens, J.R. Fredericks, S.T. Polkus, P. Sipple, A.D. Patten, D. Dexter, S. P. Seitz, J.L. Gross, Cancer Res. 54 (1994) 2199–2206.
[33] L. González-Bulnes, J. Gallego, J. Amer. Chem. Soc. 131 (2009) 7781–7791.
[34] L. González-Bulnes, J. Gallego, Biopolymers 97 (2012) 974–987.
[35] J. Gallego, B.R. Reid, Biochemistry 38 (1999) 15104–15115.
[36] S.S. Mati, S.S. Roy, S. Chall, S. Bhattacharya, S.C. Bhattacharya, J. Phys. Chem. B 117 (2013) 14655–14665.
[37] S. Banerjee, J.A. Kitchen, T. Gunnlaugsson, J.M. Kelly, Org. Biomol. Chem. 10 (2012) 3033–3043.
[38] M.S. Malik, S. Farooq Adil, Z. Moussa, H.M. Altass, I.I. Althagafi, M. Morad, M. A. Ansari, Q.M. Sajid Jamal, R.J. Obaid, A.A. Al-Warthan, T.B. Shaik, S.A. Ahmed, Front. Chem. 9 (2021) 630357.
[39] T. Mijatovic, T. Mahieu, N. De Neve, J. Dewelle, G. Simon, M.J.M. Dehoux, E. van der Aar, B. Haibe-Kains, G. Bontempi, C. Deacestecker, E. Van Quaquebeke, F. Darro, R. Kiss, Neoplasia 10 (2008) 573–586.
[40] R. Tandon, V. Luxami, N. Tandon, K. Paul, Bioorg. Chem. 121 (2022) 105677.
[41] A. Pain, S. Samanta, S. Dutta, A. Saxena, M. Shanmugavel, H. Kampasi, G. Qazi, U. Sanyal, Exp. Oncol. 24 (2002) 173–179.
[42] A. Pain, S. Samanta, S. Dutta, A.K. Saxena, M. Shanmugavel, H. Kampasi, G. N. Qazi, U. Sanyal, J. Exp. Clin. Cancer Res. 22 (2003) 411–418.
[43] T. Brider, B. Redko, M. Oron-Herman, A. Cohen-Matzlich, G. Gerlitz, G. Gellerman, F. Grynszpan, Res. Chem. Intermed. 42 (2016) 1741–1757.
[44] Q. Lou, L. Ji, W. Zhong, S. Li, S. Yu, Z. Li, X. Meng, Molecules 19 (2014) 8803–8819.
[45] S.-Q. Xie, Y.-H. Zhang, Q. Li, F.-H. Xu, J.-W. Miao, J. Zhao, C.-J. Wang, Apoptosis 17 (2012) 725–734.
[46] S. Tan, D. Sun, J. Lyu, X. Sun, F. Wu, Q. Li, Y. Yang, J. Liu, X. Wang, Z. Chen, H. Li, X. Qian, Y. Xu, Biorg, Med. Chem. 23 (2015) 5672–5680.
[47] A.S. Oshchepkov, T.A. Shumilova, M. Zerson, R. Magerle, V.N. Khrustalev, E. A. Kataev, J. Org. Chem. 84 (2019) 9034–9043.
[48] O.A. Fedorova, A.N. Arkhipova, P.A. Panchenko, J. Berthet, S. Delbaere, S. Minkovska, Y.V. Fedorov, J. Photochem. Photobiol., A 405 (2021) 112975.
[49] L.G. Alves, A. Pilon, S. Rodriguez-Calado, J.F. Portel, O. Ferreira, S.A. Sousa, A. Valente, J. Lorenzo, E.R. Silva, A.M. Martins, J.H. Leitão, In: Proceedings of the 5th International Electronic Conference on Medicinal Chemistry, Basel, Switzerland, MDPI, 2019.
[50] H.K. Hariprakasha, T. Kosakowska-Cholody, C. Meyer, W.M. Cholody, S. F. Stinson, N.I. Tarasova, C.J. Michejda, J. Med. Chem. 50 (2007) 5557–5560.
[51] Z.-J. Xu, Y.-J. Zhou, J.-H. Wang, L.-F. Mao, W. Li, G.-Q. Xu, Front. Bioeng, Biotechnol 9 (2021) 662432.
[52] A. Kamal, S.F. Adil, R.T. Jaki, B. Siddardha, U.S.N. Murthy, Lett. Drug Des. Discov. 6 (2009) 201–209.
[53] A. Wu, Y. Xu, X. Qian, Monatsh. Chem. 141 (2010) 893–899.
[54] M.F. Braña, M. Cacho, M.A. García, B. de Pascual-Teresa, A. Ramos, M. T. Domínguez, J.M. Pozuelo, C. Abradelo, M.F. Rey-Stolle, M. Yuste, M. Báñez-Coronel, J.C. Lacal, J. Med. Chem. 47 (2004) 1391–1399.
[55] C. Ge, L. Chang, Y. Zhao, C. Chang, X. Xu, H. He, Y. Wang, F. Dai, S. Xie, C. Wang, Molecules 22 (2017) 342.
[56] J.M. Herrera, F. Mendes, S. Gama, I. Santos, C. Navarro Ranninger, S. Cabrera, A. G. Quiroga, Inorg. Chem. 53 (2014) 12627–12634.
[57] Y. Li, K. Yue, L. Li, J. Niu, H. Liu, J. Ma, S. Xie, Bioorg. Chem. 101 (2020) 104011.
[58] F. Navas, F. Mendes, I. Santos, C. Navarro-Ranninger, S. Cabrera, A.G. Quiroga, Inorg. Chem. 56 (2017) 6175–6183.
[59] J.M. Pérez, I. López-Solera, E.I. Montero, M.F. Braña, C. Alonso, S.P. Robinson, C. Navarro-Ranninger, J. Med. Chem. 42 (1999) 5482–5486.
[60] K. Ghebreyessus, A. Peralta, M. Katdare, K. Prabhakaran, S. Paranawithana, Inorg. Chim. Acta 434 (2015) 239–251.
[61] D.C. Magri, A.D. Johnson, R.S.C. Med, Chem 16 (2025) 4657–4675.
[62] U. Ndagi, N. Mhlongo, M.E. Soliman, Drug Des, Devel. Ther. 11 (2017) 599–616.
[63] Y. Guo, Y. He, S. Wu, S. Zhang, D. Song, Z. Zhu, Z. Guo, X. Wang, Inorg. Chem. 58 (2019) 13150–13160.
[64] E.Y.D. Chua, G.E. Davey, C.F. Chin, P. Dröge, W.H. Ang, C.A. Davey, Nucleic Acids Res. 43 (2015) 5284–5296.
[65] J. Karges, Angew. Chem. Int. Ed. 61 (2022) e202112236.
[66] S. Banerjee, J.A. Kitchen, S.A. Bright, J.E. O'Brien, D.C. Williams, J.M. Kelly, T. Gunnlaugsson, Chem. Commun. 49 (2013) 8522–8524.
[67] Z. Ou, Y. Qian, Y. Gao, Y. Wang, G. Yang, Y. Li, K. Jiang, X. Wang, RSC Adv. 6 (2016) 36923–36931.
[68] Y. Wang, X. Shi, H. Fang, Z. Han, H. Yuan, Z. Zhu, L. Dong, Z. Guo, X. Wang, J. Med. Chem. 65 (2022) 7786–7798.
[69] X. Wang, Y. Wang, S. Gou, F. Chen, Bioorg. Chem. 104 (2020) 104210.
[70] M.V. Babak, D. Plażuk, S.M. Meier, H.J. Arabshahi, J. Reynisson, B. Rychlik, A. Błauż, K. Szulc, M. Hanif, S. Strobl, A. Roller, B.K. Keppler, C.G. Hartinger, Chem. A Eur. J. 21 (2015) 5110–5117.

[71] W.D.J. Tremlett, D.M. Goodman, T.R. Steel, S. Kumar, A. Wieczorek-Błauż, F. P. Walsh, M.P. Sullivan, M. Hanif, C.G. Hartinger, Coord. Chem. Rev. 445 (2021) 213950.
[72] T.R. Steel, J. Stjärnhage, Z. Lin, H.O. Bloomfield, C.D. Herbert, J.W. Astin, K. Krawczyk, B. Rychlik, D. Plażuk, S.M.F. Jamieson, C.G. Hartinger, Dalton Trans. 54 (2025) 1583–1596.
[73] G.-B. Liang, Y.-C. Yu, J.-H. Wei, W.-B. Kuang, Z.-F. Chen, Y. Zhang, Eur. J. Med. Chem. 188 (2020) 112033.
[74] D. Gibson, J. Inorg. Biochem. 217 (2021) 111353.
[75] C. Marotta, E. Giorgi, F. Binacchi, D. Cirri, C. Gabbiani, A. Pratesi, Inorg. Chim. Acta 548 (2023) 121388.
[76] M.H.C. Boulet, H.R. Bolland, E.M. Hammond, A.C. Sedgwick, J. Amer. Chem. Soc. 145 (2023) 12998–13002.
[77] Q. Wang, Y. Chen, G. Li, Y. Zhao, Z. Liu, R. Zhang, M. Liu, D. Li, J. Han, Bioorg. Med. Chem. Lett. 29 (2019) 126670.
[78] Z. Li, Y. Chen, Z. Liu, Q. Wang, Y. Zhao, J. Wei, M. Liu, Z. Wang, D. Li, J. Han, Monatsh. Chem. 151 (2020) 353–367.
[79] Q. Wang, X. Tan, Z. Liu, G. Li, R. Zhang, J. Wei, S. Wang, D. Li, B. Wang, J. Han, Eur. J. Pharm. Sci. 124 (2018) 127–136.
[80] Q. Wang, G. Li, Z. Liu, X. Tan, Z. Ding, J. Ma, L. Li, D. Li, J. Han, B. Wang, Eur. J. Inorg. Chem. 2018 (2018) 4442–4451.
[81] C.A. Puckett, R.J. Ernst, J.K. Barton, Dalton Trans. 39 (2010) 1159–1170.
[82] H. Shi, J. Kasparkova, C. Soulié, G.J. Clarkson, C. Imberti, O. Novakova, M. J. Paterson, V. Brabec, P.J. Sadler, Chem. A Eur. J. 27 (2021) 10711–10716.
[83] B. Hu, Y. Cao, K. Du, C. Liu, Y. Zhang, J. Yue, T. Ding, M. Yan, B. Guo, S. Chu, M. Zeng, X. Sun, X. Wu, S. Huang, C. Ma, C. Wang, Z. Tian, X. Hou, P.G. Wang, Y. Liu, J. Wang, S. Xie, J. Ma, J. Med. Chem. 68 (2025) 14239–14253.
[84] H.-Y. Chu, W. Wang, X. Chen, Y.-E. Jiang, R. Cheng, X. Qi, Z.-M. Zhong, M.-S. Zeng, X.-F. Zhu, C.-Z. Sun, Cancer Lett. 423 (2018) 105–112.
[85] F. Wu, C. Li, X. Song, L. Xie, Cell. Signal. 132 (2025) 111834.
[86] Y. Pan, Y. Yu, X. Wang, T. Zhang, Front. Immunol. 11 (2020) 583084.
[87] T.R. Steel, F. Walsh, A. Wieczorek-Błauż, M. Hanif, C.G. Hartinger, Coord. Chem. Rev. 439 (2021) 213890.
[88] G.M. O'Kane, J. Spratlin, D.Y. Oh, S.Y. Rha, E. McWhirter, E. Elimova, P. Kavan, M.K. Choi, D. Kim, R.A. Goodwin, J.R. Hecht, D.H. Koo, K. Halani, R. McAllister, M. Jones, M.D. Snow, Y. Lemmerick, G. Spera, J. Pankovich, Ann. Oncol. 35 (2024) S22.
[89] J.L. Spratlin, G.M. O'Kane, D.-Y. Oh, S.Y. Rha, E. McWhirter, E. Elimova, P. Kavan, M.K. Choi, D.W. Kim, R.A. Goodwin, J.R. Hecht, S.T. Kim, D.-H. Koo, K. Halani, E.R. McAllister, M. Jones, M. Snow, Y. Lemmerick, G. Spera, J. Pankovich, J. Clin. Oncol. 42 (2024) 143.
[90] Theralase® Technologies Inc., 2019, https://clinicaltrials.gov/study/NCT03945162.
[91] G.S. Kulkarni, K.A. Richards, P.C. Black, R.A. Rendon, J. Chin, N.D. Shore, G. Jayram, E.V. Kramolowsky, D. Saltzstein, P.K. Agarwal, L. Belkoff, M. A. O'Donnell, A.M. Kamat, M.A.S. Jewett, D.L. Lamm, V. DeGruttola, A. Mandel, R. Dumoulin-White, W. Kassouf, J. Clin. Oncol. 41 (2023) 528.
[92] J. Liu, C. Zhang, T.W. Rees, L. Ke, L. Ji, H. Chao, Coord. Chem. Rev. 363 (2018) 17–28.
[93] F.E. Poynton, S.A. Bright, S. Blasco, D.C. Williams, J.M. Kelly, T. Gunnlaugsson, Chem. Soc. Rev. 46 (2017) 7706–7756.
[94] G.J. Ryan, S. Quinn, T. Gunnlaugsson, Inorg. Chem. 47 (2008) 401–403.
[95] R.B.P. Elmes, G.J. Ryan, M.L. Erby, D.O. Frimannsson, J.A. Kitchen, M. Lawler, D. C. Williams, S.J. Quinn, T. Gunnlaugsson, Inorg. Chem. 59 (2020) 10874–10893.
[96] G.J. Ryan, F.E. Poynton, R.B.P. Elmes, M. Erby, D.C. Williams, S.J. Quinn, T. Gunnlaugsson, Dalton Trans. 44 (2015) 16332–16344.
[97] S. Monro, K.L. Colón, H. Yin, J. Roque, P. Konda, S. Gujar, R.P. Thummel, L. Lilge, C.G. Cameron, S.A. McFarland, Chem. Rev. 119 (2019) 797–828.
[98] Y. Sun, J. Li, H. Zhao, L. Tan, J. Inorg. Biochem. 163 (2016) 88–94.
[99] J. Li, Y. Sun, L. Xie, X. He, L. Tan, J. Inorg. Biochem. 143 (2015) 56–63.
[100] H. Wang, L. Chen, Z. Mao, S. Liu, R. Huang, R. He, Y. Zhang, J. Wei, J. Med. Chem. 68 (2025) 10203–10215.
[101] K.J. Kilpin, C.M. Clavel, F. Edafe, P.J. Dyson, Organometallics 31 (2012) 7031–7039.
[102] B. Mohan, S. Estalayo-Adrián, D. Umadevi, B. la Cour Poulsen, S. Blasco, G. J. McManus, T. Gunnlaugsson, S. Shanmugaraju, Inorg. Chem. 61 (2022) 11592–11599.
[103] W. Streciwilk, A. Terenzi, F. Lo Nardo, P. Prochnow, J.E. Bandow, B.K. Keppler, I. Ott, Eur. J. Inorg. Chem. 2018 (2018) 3104–3112.
[104] W. Streciwilk, A. Terenzi, X. Cheng, L. Hager, Y. Dabiri, P. Prochnow, J. E. Bandow, S. Wölfl, B.K. Keppler, I. Ott, Eur. J. Med. Chem. 156 (2018) 148–161.
[105] W. Streciwilk, A. Terenzi, R. Misgeld, C. Frias, P.G. Jones, A. Prokop, B. K. Keppler, I. Ott, ChemMedChem 12 (2017) 214–225.
[106] A. Meyer, L. Oehninger, Y. Geldmacher, H. Alborzinia, S. Wölfl, W.S. Sheldrick, I. Ott, ChemMedChem 9 (2014) 1794–1800.
[107] L.M. Groves, C.F. Williams, A.J. Hayes, B.D. Ward, M.D. Isaacs, N.O. Symonds, D. Lloyd, P.N. Horton, S.J. Coles, S.J.A. Pope, Dalton Trans. 48 (2019) 1599–1612.
[108] S. Sen, M.W. Perrin, A.C. Sedgwick, E.Y. Dunsky, V.M. Lynch, X.-P. He, J. L. Sessler, J.F. Arambula, Chem. Commun. 56 (2020) 7877–7880.
[109] C.P. Bagowski, Y. You, H. Scheffler, D.H. Vlecken, D.J. Schmitz, I. Ott, Dalton Trans. (2009) 10799–10805.
[110] R.B.P. Elmes, M. Erby, S.A. Bright, D.C. Williams, T. Gunnlaugsson, Chem. Commun. 48 (2012) 2588–2590.
[111] S.A. Bright, M. Erby, F.E. Poynton, D. Monteyne, D. Pérez-Morga, T. Gunnlaugsson, D.C. Williams, R.B.P. Elmes, R.S.C. Chem, Biol 5 (2024) 344–359.
[112] F. Bisceglie, G. Pelosi, N. Orsoni, M. Pioli, M. Carcelli, P. Pelagatti, S. Pinelli, P. J. Sadler, Int. J. Mol. Sci. 23 (2022).
[113] W. Ma, S. Zhang, Z. Tian, Z. Xu, Y. Zhang, X. Xia, X. Chen, Z. Liu, Eur. J. Med. Chem. 181 (2019) 111599.
[114] P. Srivastava, M. Verma, A. Kumar, P. Srivastava, R. Mishra, S. Sivakumar, A. K. Patra, Dalton Trans. 50 (2021) 3629–3640.
[115] S. Shanmugaraju, B. la Cour Poulsen, T. Arisa, D. Umadevi, H.L. Dalton, C. S. Hawes, S. Estalayo-Adrián, A.J. Savyasachi, G.W. Watson, D.C. Williams, T. Gunnlaugsson, Chem. Commun. 54 (2018) 4120–4123.
[116] T. Esatbeyoglu, P. Huebbe, I.M.A. Ernst, D. Chin, A.E. Wagner, G. Rimbach, Angew. Chem. Int. Ed. 51 (2012) 5308–5332.
[117] L. Shen, H.-F. Ji, Trends in Mol. Med. 18 (2012) 138–144.
[118] F. Caruso, M. Rossi, A. Benson, C. Opazo, D. Freedman, E. Monti, M.B. Gariboldi, J. Shaulky, F. Marchetti, R. Pettinari, C. Pettinari, J. Med. Chem. 55 (2012) 1072–1081.
[119] R. Pettinari, F. Marchetti, F. Condello, C. Pettinari, G. Lupidi, R. Scopelliti, S. Mukhopadhyay, T. Riedel, P.J. Dyson, Organometallics 33 (2014) 3709–3715.
[120] B. Mohan, A. Jose, I. Bhattacharjee, R. Saravanan, M.K. Noushija, M. Porel, B. R. Sarangi, S. Shanmugaraju, Dalton Trans. 54 (2025) 10549–10557.
[121] T. Topală, A. Bodoki, L. Oprean, R. Oprean, Med. Pharm. Rep. 87 (2014) 215–219.
[122] S. Blanck, T. Cruchter, A. Vultur, R. Riedel, K. Harms, M. Herlyn, E. Meggers, Organometallics 30 (2011) 4598–4606.
[123] R. Roskoski, Pharmacol. Res. 200 (2024) 107059.
[124] Y. Dabiri, A. Schmid, J. Theobald, B. Blagojevic, W. Streciwilk, I. Ott, S. Wölfl, X. Cheng, Int. J. Mol. Sci. 19 (2018) 3964.
[125] F. Battistin, G. Balducci, E. Iengo, N. Demitri, E. Alessio, Eur. J. Inorg. Chem. 2016 (2016) 2850–2860.
[126] K. Gaur, A.M. Vázquez-Salgado, G. Duran-Camacho, I. Dominguez-Martinez, J. A. Benjamín-Rivera, L. Fernández-Vega, L.C. Sarabia, A.C. García, F. Pérez-Deliz, J.A. Méndez Román, M. Vega-Cartagena, S.A. Loza-Rosas, X.R. Acevedo, A.D. Tinoco, Inorganics, 6, 2018.
[127] S.A. Shaikh, S.S. Bhat, V.K. Revankar, N.S.K. Kumara, N.K. Lokanath, R. J. Butcher, V. Kumbar, K. Bhat, New J. Chem. 46 (2022) 16801–16812.
[128] S.A. Shaikh, S.S. Bhat, P.L. Hegde, V.K. Revankar, A. Kate, D. Kirtani, A. A. Kumbhar, V. Kumbar, K. Bhat, New J. Chem. 45 (2021) 16319–16332.
[129] S.A. Shaikh, S.S. Bhat, V.K. Revankar, S. Naveen, N.K. Mahesha, V. Kumbar Lokanath, Inorg, Chim. Acta 559 (2024) 121799.
[130] K. Wang, L. Wang, Z. Shang, X. Yang, H. Li, X. Wang, M. Zhu, Q. Meng, J. Inorg. Biochem. 261 (2024) 112721.
[131] K. Wang, L. Wang, H. Li, X. Yang, Z. Shang, Q. Han, X. Wang, Q. Meng, M. Zhu, J. Mol. Struct. 1327 (2025) 141184.
[132] S. Ghosh, R. Saha, S. Sarkar, A. Biswas, K. Ghosh, Spectrochim. Acta A: Mol. Biomol, Spectrosc 305 (2024) 123428.
[133] S. Roy, S. Saha, R. Majumdar, R.R. Dighe, A.R. Chakravarty, Inorg. Chem. 48 (2009) 9501–9509.
[134] N. Tyagi, M. Viji, S.C. Karunakaran, S. Varughese, S. Ganesan, S. Priya, P. S. Saneesh Babu, A.S. Nair, D. Ramaiah, Dalton Trans. 44 (2015) 15591–15601.
[135] S.Z. Topal, Ş.Ş. Ün, Y. Bretonnière, S.T. Kostakoğlu, J. Photochem. Photobiol. A Chem. 332 (2017) 562–570.
[136] T. Küçük, K. Harmandar, M.S. Yalçın, Ş.Ş. Ün, S.T. Kostakoğlu, İ.N. Zengin, E. N. Kaya, S. Özdemir, D. Atilla, Polyhedron 261 (2024) 117113.
[137] S. Wang, P. Huang, X. Chen, Adv. Mater. 28 (2016) 7340–7364.
[138] M. Yang, S. Cao, X. Sun, H. Su, H. Li, G. Liu, X. Luo, F. Wu, Bioconjug. Chem. 31 (2020) 663–672.
[139] M. Cui, S. Zhu, M. Xiong, H. Zuo, X. Li, K. Wang, J. Jiang, J. Porphyrins Phthalocyanines 28 (2024) 166–172.
[140] Y. Matsumura, H. Maeda, Cancer Res. 46 (1986) 6387–6392.
[141] S. Tan, K. Han, Q. Li, L. Tong, Y. Yang, Z. Chen, H. Xie, J. Ding, X. Qian, Y. Xu, Eur. J. Med. Chem. 85 (2014) 207–214.
[142] Q. Li, T.A. van den Berg, B.L. Feringa, G. Roelfes, Dalton Trans. 39 (2010) 8012–8021.
[143] I. Grabchev, D. Staneva, E. Vasileva-Tonkova, R. Alexandrova, M. Cangiotti, A. Fattori, M.F. Ottaviani, J. Polym. Res. 24 (2017) 210.
[144] I. Grabchev, D. Staneva, E. Vasileva-Tonkova, R. Alexandrova, Chemosensors 7 (2019) 17.
[145] D. Staneva, A.I. Said, P. Grozdanov, I. Nikolova, R. Stoyanova, A. Jordanova, I. Grabchev, Photochem. Photobiol. Sci. 24 (2025) 593–606.
[146] D. Staneva, E. Vasileva-Tonkova, P. Bosch, P. Grozdanov, I. Grabchev, Macromol. Res. 26 (2018) 332–340.
[147] A.I. Said, D. Staneva, E. Vasileva-Tonkova, P. Grozdanov, I. Nikolova, R. Stoyanova, A. Jordanova, I. Grabchev, Chemosensors 12 (2024) 79.
[148] M. Cangiotti, D. Staneva, M.F. Ottaviani, E. Vasileva-Tonkova, I. Grabchev, J. Photochem. Photobiol., A 415 (2021) 113312.
[149] B. Canonico, M. Cangiotti, M. Montanari, S. Papa, V. Fusi, L. Giorgi, C. Ciacci, M. F. Ottaviani, D. Staneva, I. Grabchev, Biol. Chem. 403 (2022) 345–360.
[150] H. Manov, D. Staneva, E. Vasileva-Tonkova, R. Kukeva, S. Stoyanov, I. Grabchev, R. Alexandrova, R. Stoyanova, Biointerface Res. Appl. Chem. 12 (2022) 5534–5547.
[151] C. Maher, A. Hassan Karl, mBio 14 (2023) e01205–01223.
[152] B. Stiller, S. Hager, N.R. Filipović, C.R. Kowol, P. Heffeter, Future, Med. Chem. 17 (2025) 2425–2428.
[153] H. Sharma, N. Kaur, N. Singh, Inorg. Chim. Acta 391 (2012) 83–87.

[154] S.A. Shaikh, S.S. Bhat, V.K. Revankar, N.S. Mahesha, N.K. Loknath, V. Kumbar, J. Coord. Chem. 76 (2023) 1586–1603.
[155] J. Nekvinda, D. Różycka, S. Rykowski, E. Wyszko, A. Fedoruk-Wyszomirska, D. Gurda, M. Orlicka-Płocka, M. Giel-Pietraszuk, A. Kiliszek, W. Rypniewski, R. Bachorz, J. Wojcieszak, B. Grüner, A.B. Olejniczak, Bioorg. Chem. 94 (2020) 103432.
[156] A. Bogucka-Kocka, P. Kołodziej, A. Makuch-Kocka, D. Różycka, S. Rykowski, J. Nekvinda, B. Grüner, A.B. Olejniczak, Chem. Commun. 58 (2022) 2528–2531.
[157] P. Chellan, P.J. Sadler, Chem. A Eur. J. 26 (2020) 8676–8688.
[158] A. Kondratskyi, K. Kondratska, F. Vanden Abeele, D. Gordienko, C. Dubois, R.-A. Toillon, C. Slomianny, S. Lemière, P. Delcourt, E. Dewailly, R. Skryma, C. Biot, N. Prevarskaya, Sci. Rep. 7 (2017) 15896.
[159] D.-G. Jia, J.-A. Zheng, Y.-R. Fan, J.-Q. Yu, X.-L. Wu, B.-J. Wang, X.-B. Yang, Y. Huang, J. Organomet. Chem. 888 (2019) 16–23.
[160] J.-L. Butour, J.-P. Macquet, Biochim., Biophys, Acta, Nucleic Acids Protein Synth. 653 (1981) 305–315.
[161] S. Satyanarayana, J.C. Dabrowiak, J.B. Chaires, Biochemistry 32 (1993) 2573–2584.
[162] Y.-R. Fan, B.-J. Wang, D.-G. Jia, X.-B. Yang, Y. Huang, J. Inorg. Biochem. 219 (2021) 111425.
[163] A.D. Johnson, J.A. Buhagiar, D.C. Magri, R.S.C. Med, Chem 12 (2021) 2060–2064.
[164] X. Li, H. Wang, Y. Zhang, Q. Cao, Y. Chen, Chin. Chem. Lett. 32 (2021) 1541–1544.
[165] G.-J.-S. Cheng, J.-M. Qin, X. Li, Q.-Y. Cao, Dyes Pigments 211 (2023) 111089.
[166] U.R. Gandra, B. Jana, P. Hammer, M.I.H. Mohideen, U. Neugebauer, A. Schiller, Chem. Commun. 60 (2024) 2098–2101.
[167] U. Schatzschneider, Br. J. Pharmacol. 172 (2015) 1638–1650.
[168] I. Grabchev, S. Yordanova, P. Bosch, E. Vasileva-Tonkova, R. Kukeva, S. Stoyanov, R. Stoyanova, J. Mol. Struct. 1130 (2017) 974–983.
[169] C.G. Hartinger, N. Metzler-Nolte, P.J. Dyson, Organometallics 31 (2012) 5677–5685.
[170] K. Peng, Y. Zheng, W. Xia, Z.-W. Mao, Chem. Soc. Rev. 52 (2023) 2790–2832.
[171] C. Roder, M.J. Thomson, Drugs R&D 15 (2015) 13–20.
[172] D. Giorgini, L. Chiaverini, M. Viviano, R. Belvedere, S. Salerno, E. Baglini, F. Da Settimo, T. Marzo, S. Taliani, E. Barresi, Pharmaceuticals 18 (2025) 1628.
[173] A. Jatoi, N.R. Foster, A. Wahner Hendrickson, M.S. Block, S.J. Weroha, E. J. Asmus, N.R. Murray, A.P. Fields, Am. J. Clin. Oncol. (2025).
[174] M.E. Hoffmann, F.E. Kühn, Chem. Soc. Rev. 54 (2025) 10326–10343.
[175] A. Pratesi, C. Gabbiani, E. Michelucci, M. Ginanneschi, A.M. Papini, R. Rubbiani, I. Ott, L. Messori, J. Inorg. Biochem. 136 (2014) 161–169.
[176] I. Ott, X. Qian, Y. Xu, D.H.W. Vlecken, I.J. Marques, D. Kubutat, J. Will, W. S. Sheldrick, P. Jesse, A. Prokop, C.P. Bagowski, J. Med. Chem. 52 (2009) 763–770.
[177] A. Kumari, R.K. Singh, Bioorg. Chem. 96 (2020) 103578.
[178] J. Zhao, S. Sun, X. Li, W. Zhang, S. Gou, A.C.S. Appl, Bio Mater. 3 (2020) 252–262.
[179] S. He, F.A. Alhumaydhi, W. Al Abdulmonem, M.A. Aljasir, M. Ibrahim, Coord, Chem. Rev. 534 (2025) 216582.
[180] X. Xiao, J. Liang, J. Xie, X. Liu, D. Zhu, Y. Dong, J. Mol. Struct. 1146 (2017) 233–241.